Chapter 9
Feedback Electronic Circuits

Several important applications of feedback systems to designing electronic circuits are presented in this chapter. Some of these applications are employed in designing some of the control systems to be presented in subsequent chapters in this book. Some other applications, such as those of oscillator circuits, constitute by themselves complete control systems requiring the employment of the control theory concepts introduced in the previous chapters.

9.1 Reducing the Effects of Nonlinearities in Electronic Circuits

Consider the closed-loop system depicted in Fig. 9.1. The corresponding closed-loop transfer function is:

$$\frac{C(s)}{R(s)} = \frac{A}{1+\beta A},$$

where A and β are positive constants. Suppose that $\beta A \gg 1$, then:

$$\frac{C(s)}{R(s)} = \frac{A}{1+\beta A} \approx \frac{1}{\beta}. \tag{9.1}$$

The applications of this fact are important in electronic circuits, as explained in the following.

Suppose that A is the gain of a power amplifier. These devices are capable of handling large amounts of power; hence, their components must be capable of working under large temperature variations. This implies that the components of a power amplifier are not high-precision and large changes in their parameters

V. M. Hernández-Guzmán, R. Silva-Ortigoza, *Automatic Control with Experiments*,
Advanced Textbooks in Control and Signal Processing,
https://doi.org/10.1007/978-3-319-75804-6_9

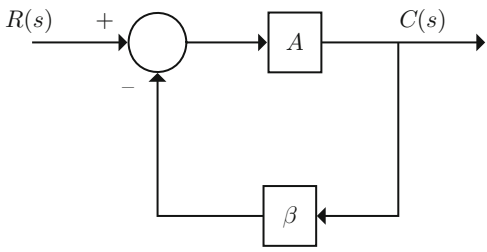

Fig. 9.1 Closed-loop system

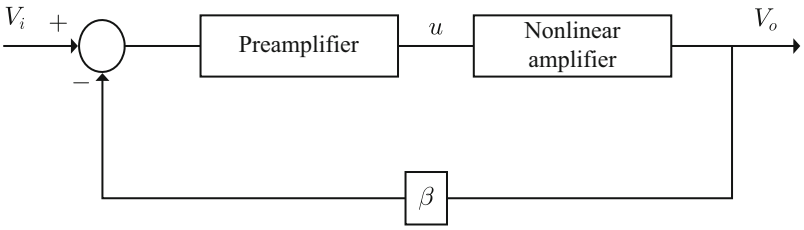

Fig. 9.2 Use of feedback in a nonlinear amplifier to reduce distortion

are expected. Thus, it is natural to assume that A changes under normal operation conditions. According to (9.1), the use of feedback around an amplifier with gain A has the effect of rendering the circuit gain changes small, despite A exhibiting large variations. Hence, feedback can solve the problem of a power amplifier with large gain changes. An important feature is that the gain β must not exhibit significant changes and this is achieved if such a gain depends only on low-power components, i.e., that they can be composed only of precision devices.

In the following, some applications are presented where feedback is used to reduce the gain variations in some electronic circuits, which can also be understood as the reduction of the effects of the circuit nonlinearities.

9.1.1 Reducing Distortion in Amplifiers

Consider the block diagram in Fig. 9.2. The nonlinear amplifier is an amplifier with gain $A_1 = 2$ when the input voltage u is negative and a gain $A_2 = 0.5$ when the input voltage is positive. This property can be represented as in Fig. 9.3. Hence, this amplifier delivers at its output a distorted version of the signal applied at its input. In Fig. 9.4, the signal at the nonlinear amplifier output is shown, when a sinusoidal signal is applied at its input. This is a good example of distortion. Combining the effect of all amplifiers in the direct path, it is concluded that the block diagram in Fig. 9.2 can be represented by a block diagram such as that in Fig. 9.1 where:

$$A = A_1 A_0, \quad u < 0,$$

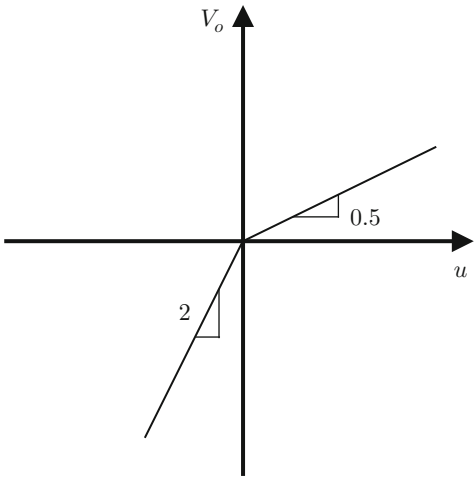

Fig. 9.3 Characteristics of the nonlinear amplifier in Fig. 9.2

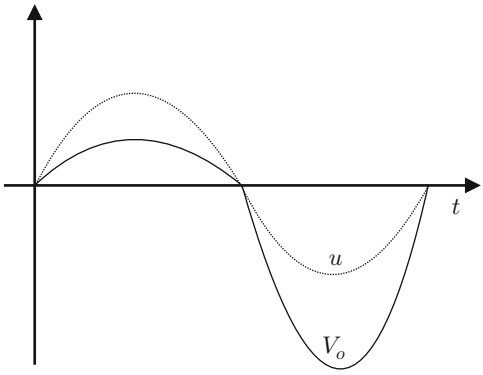

Fig. 9.4 Voltages at the input u and the output V_o of the nonlinear amplifier in Fig. 9.3

$$A = A_2 A_0, \quad u > 0,$$
$$\beta = 1, \quad \text{for instance,}$$

with A_0 the gain of the preamplifier, which is very large. Note that the following closed-loop transfer function is obtained:

$$\frac{C(s)}{R(s)} = \frac{A}{1 + \beta A} \approx \frac{1}{\beta} = 1,$$

if gains A_0 and β are such that $\beta A \gg 1$ for both values A_1, A_2. Hence, the closed-loop circuit in Fig. 9.2 works as an amplifier with constant gain β for both signs of the signal to be amplified. This means that the distortion due to the different amplifier gains A_1 and A_2 has been eliminated. This is the main advantage of feedback shown in Fig. 9.2 despite the total gain of the amplifier now being changed to $1/\beta = 1$. In Fig. 9.5, the waveform obtained for V_o at the output of the feedback

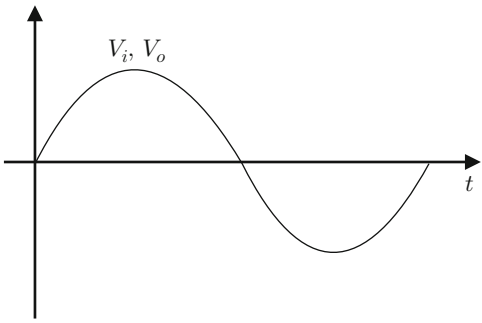

Fig. 9.5 Voltages at the input V_i and the output V_o in Fig. 9.2

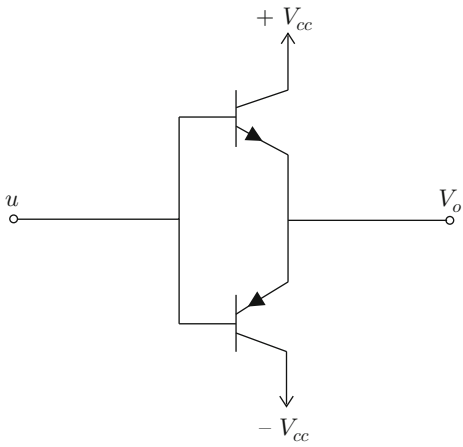

Fig. 9.6 A complementary symmetry nonlinear power amplifier

system depicted in Fig. 9.2 is shown when V_i is a sinusoidal signal. Note that V_o has the same amplitude for both semicircles when a nonlinear amplifier (with gain A) is embedded in the feedback system.

9.1.2 Dead Zone Reduction in Amplifiers

A power amplifier implemented using two transistors connected in complementary symmetry is shown in Fig. 9.6. This circuit has a dead zone between -0.6[V] and $+0.6$ [V] due to the polarization voltage level required by the base-emitter transistor junctions. This means that the output signal V_o remains at zero as long as the input signal u remains within the range $[-0.6, +0.6]$[V]. In Fig. 9.7, the characteristic of this nonlinear amplifier is shown. In Fig. 9.8, the signal obtained at the amplifier output V_o is shown, when a sinusoidal signal is applied at the input u. Note the effect of the dead zone for values of u that are close to zero. The circuit in Fig. 9.9 is employed to reduce the effect of such a dead zone. The objective is to render the waveform at the output V_o identical or very similar to the waveform of the applied

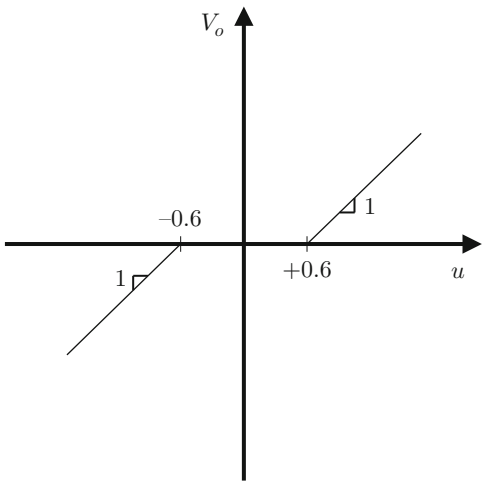

Fig. 9.7 Characteristics of the nonlinear amplifier in Fig. 9.6

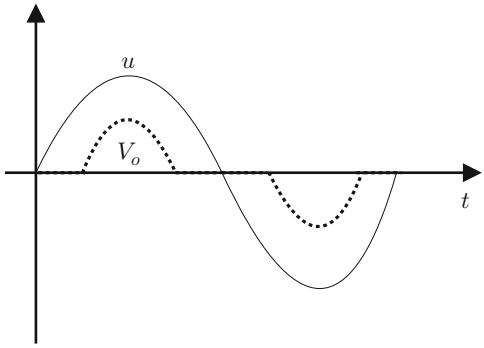

Fig. 9.8 Voltages at the input u and the output V_o of the amplifier in Fig. 9.6

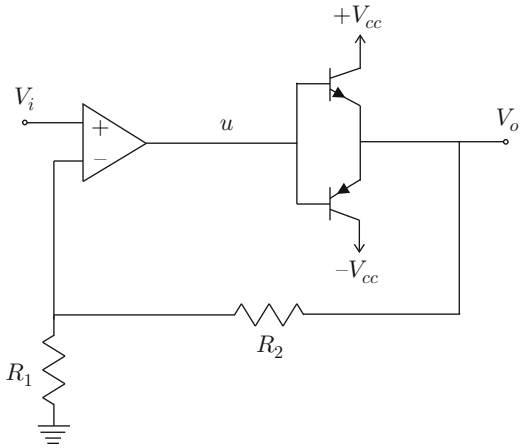

Fig. 9.9 Feedback circuit to reduce the effect of the nonlinearity present in the amplifier in Fig. 9.6

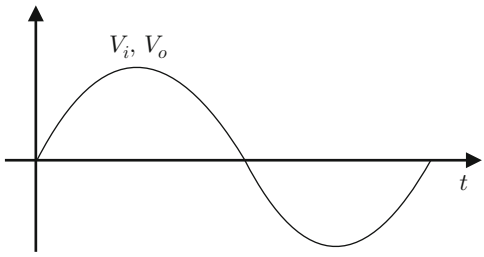

Fig. 9.10 Voltages at the input V_i and the output V_o of the circuit in Fig. 9.9

signal V_i, as shown in Fig. 9.10; hence, to eliminate the effect of the dead zone by employing feedback. This is explained as follows.

The circuit in Fig. 9.9 can be represented by the block diagram in Fig. 9.1. This feedback system has a closed-loop transfer function given as:

$$\frac{C(s)}{R(s)} = \frac{A}{1+\beta A}, \quad C(s) = V_o(s), \quad R(s) = V_i(s),$$
$$\beta = \frac{R_1}{R_1 + R_2} \leq 1,$$

where $A = \alpha(u)A_0$, with A_0 the open-loop transfer function of the operational amplifier used to implement the subtraction point and $\alpha(u)$ is the u dependent gain of the characteristic shown in Fig. 9.7, i.e., the dead zone can be represented as $V_o = \alpha(u)u$. It is well known that A_0 is a large real scalar, in the order of 100,000, whereas $\alpha(u)$ has a value in the open interval (0, 1]. Recall that the dead zone is an idealized *hard* behavior of the real smooth behavior of a transistor. Thus, $\beta A = \alpha(u)A_0\beta \gg 1$ and the following can be approximated, with a small error:

$$\frac{V_o(s)}{V_i(s)} = \frac{A}{1+\beta A} \approx \frac{1}{\beta}. \tag{9.2}$$

The expression in (9.2) indicates that the whole circuit behaves as an amplifier with the constant gain $1/\beta$ such that the effect of the dead zone is eliminated and the waveform of V_o is identical to that of V_i.

Note that R_1 and R_2 can be chosen to be large to ensure that only a small electric current flows through them; hence, precision resistances can be employed. It is also important to stress the following. According to Fig. 9.7 $\alpha(u)$ is zero for u in the interval $[-0.6, +0.6]$[V]. This suggests that the condition $\beta A = \alpha(u)A_0\beta \gg 1$ is not true. However, it is important to understand that the characteristic in Fig. 9.7 is an idealization of what really happens in practice where V_o is zero only when u is also zero.

In Fig. 9.11 the experimental voltages u and V_o corresponding to Fig. 9.6 are shown. The Darlington transistors TIP 141 (NPN) and TIP 145 (PNP) are employed. This means that the voltage at the base-emitter junction has a nominal direct polarization voltage of about 1.2[V]; hence, the dead zone is in this case in the

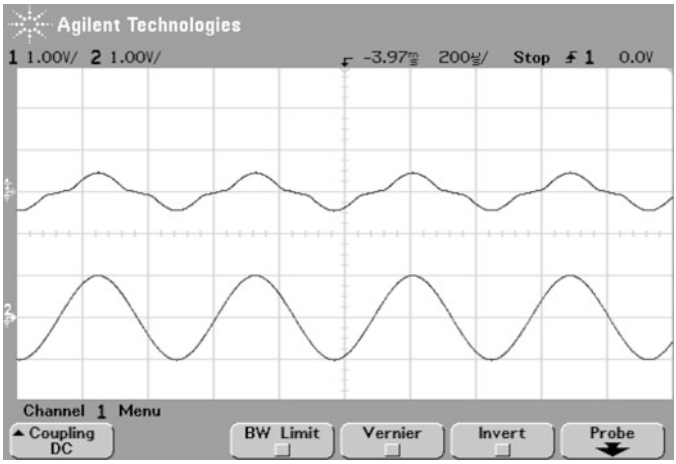

Fig. 9.11 Experimental results. Voltages at the input and the output of the circuit in Fig. 9.6. Upper line: V_o, bottom line: u

interval $[-1.2, +1.2]$[V] of voltage at the input u. Voltage u is a sinusoidal voltage at 2.083[KHz] and a peak amplitude of 1[V]. Thus, voltage at the base-emitter junction is clearly below its direct polarization nominal value. It is important to state that a 1[KOhm] resistance is used as the load between the connection of both emitters and the ground. Note that the voltage V_o has a waveform that is very different from the waveform of a sinusoidal signal (compare with the dotted line in Fig. 9.8). This experimentally verifies that the complementary symmetry connection of two transistors strongly distorts the input signal.

In Fig. 9.12, the waveforms of the signals V_i and V_o corresponding to Fig. 9.9 are shown. These measurements were obtained in an experiment where the Darlington transistors TIP 141 (NPN) and TIP 145 (PNP) are employed and voltage V_i is a sinusoidal signal at 2.083[KHz] with a peak amplitude of 1[V]. The resistances $R_1 = R_2 = 10$[KOhm] are also employed, in addition to a 1[KOhm] load resistance between the connection of both emitters and the ground. A TL081 operational amplifier is used. Note that the waveform of V_o is similar to that of V_i, i.e., both signals are sinusoidal signals of the same frequency, although the amplitude of V_o is twice the amplitude of V_i.This is because, according to (9.2):

$$\frac{V_o(s)}{V_i(s)} = \frac{1}{\beta} = 2, \quad \beta = \frac{R_1}{R_1 + R_2} = 0.5.$$

Some other applications of feedback in electronic circuits are presented in [1].

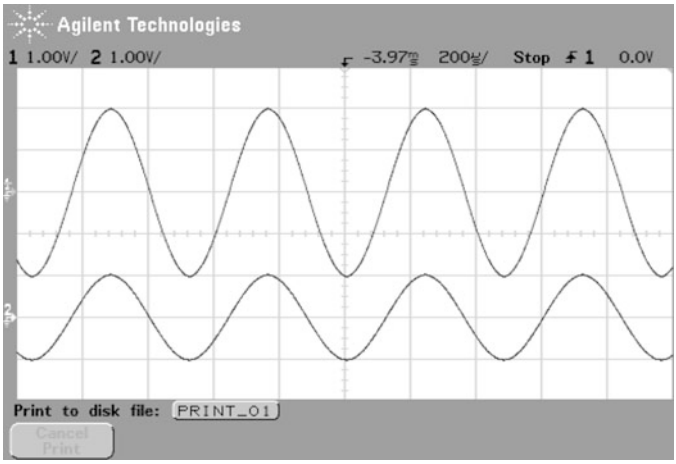

Fig. 9.12 Experimental results. Voltages at the input and the output of the circuit in Fig. 9.9. Upper line: V_o, bottom line: V_i

Fig. 9.13 Implementation of an analog controller using an operational amplifier

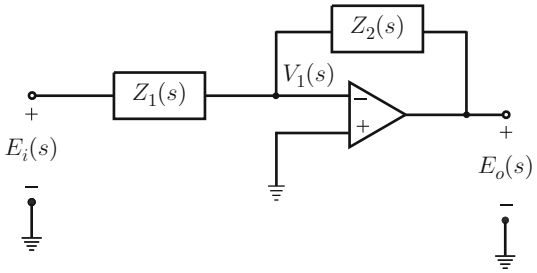

9.2 Analog Controllers with Operational Amplifiers

Consider the circuit in Fig. 9.13 where $Z_1(s)$ and $Z_2(s)$ stand for the impedances of two passive networks located at those places. In an operational amplifier, it is true that:

$$E_o(s) = (V_+(s) - V_-(s))A_0,$$

where $V_+(s)$ and $V_-(s)$ stand respectively for voltages at the terminals "+" and "−" of the operational amplifier, whereas A_0 is the open-loop gain of the operational amplifier, which is very large (about 100,000 [2], pp. 500). As $V_+(s) = 0$ and $V_-(s) = V_1(s)$, then:

$$E_o(s) = (0 - V_1(s))A_0 = -V_1(s)A_0. \tag{9.3}$$

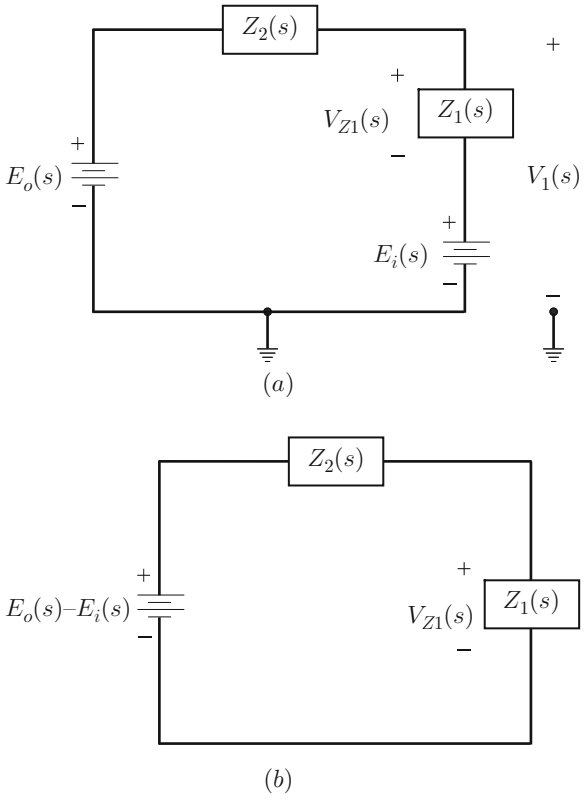

Fig. 9.14 Equivalent circuit to that shown in Fig. 9.13

To compute V_1, the auxiliary circuits in Figs. 9.14a and b are employed. There, it is found that:

$$\begin{aligned} V_1(s) &= \frac{Z_1(s)}{Z_1(s)+Z_2(s)}(E_o(s)-E_i(s))+E_i(s), \\ &= \frac{Z_1(s)}{Z_1(s)+Z_2(s)}E_o(s)+E_i(s)\left(1-\frac{Z_1(s)}{Z_1(s)+Z_2(s)}\right). \end{aligned}$$

Using (9.3), the following is found:

$$E_o(s) = -\left[\frac{Z_1(s)}{Z_1(s)+Z_2(s)}E_o(s)+E_i(s)\left(1-\frac{Z_1(s)}{Z_1(s)+Z_2(s)}\right)\right]A_0,$$

hence:

$$\frac{E_o(s)}{E_i(s)} = \frac{-A_0\left(1-\frac{Z_1(s)}{Z_1(s)+Z_2(s)}\right)}{1+A_0\frac{Z_1(s)}{Z_1(s)+Z_2(s)}}.$$

Rearranging the terms:

$$\frac{E_o(s)}{E_i(s)} = \frac{-A_0\left(\frac{Z_2(s)}{Z_1(s)+Z_2(s)}\right)}{1+A_0\frac{Z_1(s)}{Z_1(s)+Z_2(s)}}.$$

It is possible to assume that $A_0\frac{Z_1(s)}{Z_1(s)+Z_2(s)} \gg 1$, because A_0 is very large; thus:

$$\frac{E_o(s)}{E_i(s)} = -\frac{Z_2(s)}{Z_1(s)}. \tag{9.4}$$

Note, however, that the condition $A_0\frac{Z_1(s)}{Z_1(s)+Z_2(s)} \gg 1$ is true depending on A_0. In this respect, it is important to point out that, in practical operational amplifiers, the gain A_0 is not a constant, but changes with the frequency of the signals the operational amplifier is processing. It is common that A_0 decreases when such a frequency increases in a similar manner to the magnitude of a low-pass filter [2], pp. 500. Hence, the conditions $A_0\frac{Z_1(s)}{Z_1(s)+Z_2(s)} \gg 1$ and (9.4) are not satisfied for high frequencies. On the other hand, the manner in which A_0 changes with the frequency depends on the particular operational amplifier that is employed. This means that attention must be paid when selecting an operational amplifier for a given application, i.e., taking into account how fast the plant to be controlled is.

In Table 9.1, some examples are shown on the possible networks employed to implement $Z_1(s)$ and $Z_2(s)$, in addition to the analog controller that results when using them. It is left as an exercise for the reader to compute $Z_1(s)$ and $Z_2(s)$ for each one of these networks to verify, using (9.4), that the transfer function of the controller in the column at the right of this table is obtained. See [3] for a more complete table including additional controllers. It is stressed, however, that these controllers can also be implemented using either a digital computer or a microcontroller.

Table 9.1 Implementation of analog controllers

Controller	$Z_1(s)$	$Z_2(s)$	$-\frac{Z_2(s)}{Z_1(s)}$
PI	R_1	R_2, C series	$-\frac{R_2}{R_1}\frac{\left(s+\frac{1}{R_2C}\right)}{s}$
PD	R_1, C parallel	R_2	$-R_2C\left(s+\frac{1}{R_1C}\right)$
PID	R_1, C_1 parallel	R_2, C_2 series	$-\left[\left(\frac{R_2}{R_1}+\frac{C_1}{C_2}\right)+R_2C_1s+\frac{\frac{1}{R_1C_2}}{s}\right]$
Lead compensator	R_1, C_1 parallel	R_2, C_2 parallel	$-\frac{C_1}{C_2}\frac{\left(s+\frac{1}{R_1C_1}\right)}{\left(s+\frac{1}{R_2C_2}\right)}$, $R_1C_1 > R_2C_2$

9.3 Design of Sinusoidal Waveform Oscillators

The purpose of this section is to show how control theory can be employed to design feedback electronic circuits generating sinusoidal signals. As sustained oscillations are present only in marginally stable systems, a necessary requirement for these feedback electronic circuits, from the linear control theory point of view, is that their characteristic polynomial must possess a pair of imaginary conjugate roots, i.e., the closed-loop system has to possess imaginary conjugate poles. This is known as the oscillation condition. Once this is achieved, the oscillation frequency, in radians/second, is equal to the imaginary part of such roots or poles. This part of the oscillator electronic circuit analysis and the design is performed using both classical control theory approaches: the time response and the frequency response. In the present section, some designs are presented based on either operational amplifiers or transistors.

An oscillator based on operational amplifiers simplifies the analysis and design from the control point of view and it is useful when operating at low frequencies as it avoids the necessity for inductance. It is important to stress that inductances required to generate low-frequency oscillations are large, resulting in bulky designs. The main drawback of this design is that it cannot work at high frequencies as in the radiofrequency bands because of the limitations of operational amplifiers.

On the other hand, the use of transistors results in a more complex analysis and design from the control point of view. However, the main advantage of the use of transistors is that it makes it possible to design oscillators for high frequencies, i.e., for the radiofrequency bands. The use of transistors is also interesting because of the following feature. As shown in the remainder of this section, that when operational amplifiers are employed, the resulting circuit is linear, requiring the introduction, in an artificial manner, of a nonlinear circuit component to render the oscillation possible. On the contrary, as the transistor is a nonlinear device it renders the oscillation possible in a rather natural manner.

9.3.1 Design Based on an Operational Amplifier: The Wien Bridge Oscillator

Consider the circuit in Fig. 9.15. In Example 2.14, Chap. 2, it was found that the voltages $E_o(s)$ and $E_i(s)$ are related as in (2.73). This expression is rewritten here for ease of reference:

$$\frac{E_o(s)}{E_i(s)} = G_T(s) = \frac{Ts}{T^2s^2 + 3Ts + 1}, \quad T = RC. \tag{9.5}$$

Consider now the circuit in Fig. 9.16 where an operational amplifier-based non-inverter amplifier is included, see Fig. 9.17. In the operational amplifier:

$$V_0(s) = (V_+(s) - V_-(s))A_0,$$

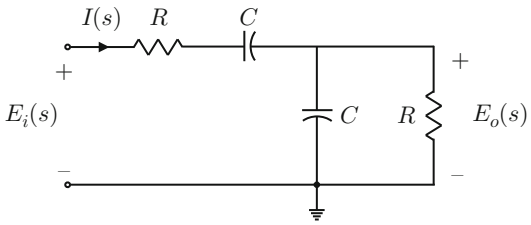

Fig. 9.15 *RC* Series parallel circuit

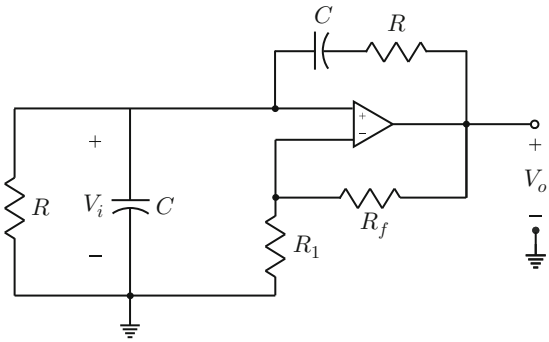

Fig. 9.16 An operational amplifier-based oscillator circuit

with $V_+(s) = V_i(s)$ and $V_-(s) = \frac{R_1}{R_1+R_f} V_0(s)$. Then:

$$V_0(s) = \left(V_i(s) - \frac{R_1}{R_1 + R_f} V_0(s) \right) A_0,$$

and rearranging:

$$V_0(s) \left(\frac{R_1 + R_f + R_1 A_0}{R_1 + R_f} \right) = A_0 V_i(s).$$

as A_0 is large, then:

$$V_0(s) \left(\frac{R_1 A_0}{R_1 + R_f} \right) = A_0 V_i(s),$$

and, finally:

$$V_0(s) = A V_i(s), \quad A = \frac{R_1 + R_f}{R_1}.$$

Note that the block diagrams in Figs. 9.18a and b can be obtained from this circuit. It is important to observe that, according to these block diagrams, the circuit in Fig. 9.16 is a positive feedback circuit. As the theory presented in the previous chapters assumes that negative feedback control systems are designed, such as that

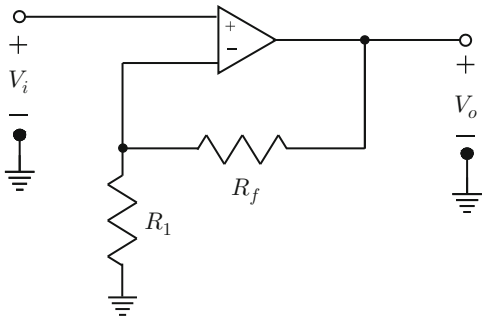

Fig. 9.17 Non-inverter amplifier

in Fig. 9.18d, it is necessary to transform the block diagram in Fig. 9.18b into a more convenient form. This is achieved in Fig. 9.18c where a negative sign is included in the feedback path, which is compensated for by a sign change in the transfer function on the direct path. Thus, a negative feedback system has been obtained that is equivalent to the systems in Figs. 9.18b and d. Thus, the open-loop transfer function is given as:

$$G(s)H(s) = -G_T(s)A. \tag{9.6}$$

9.3.2 Time Response-Based Analysis

This method studies the circuit at hand through the location of the closed-loop poles. From the study of differential equations in Chap. 3, it is known that sustained oscillations are possible only if the closed-loop poles are imaginary, i.e., with a zero real part. Under these conditions, the oscillation frequency, in radians/second, is equal to the imaginary part of these poles.

It is also known that the closed-loop poles satisfy:

$$1 + G(s)H(s) = 0.$$

Replacing (9.6) and (9.5):

$$1 + G(s)H(s) = 1 - G_T(s)A = 1 - \frac{TAs}{T^2s^2 + 3Ts + 1},$$
$$= \frac{T^2s^2 + 3Ts + 1 - TAs}{T^2s^2 + 3Ts + 1} = 0,$$

; hence, closed-loop poles satisfy:

$$T^2s^2 + (3 - A)Ts + 1 = 0.$$

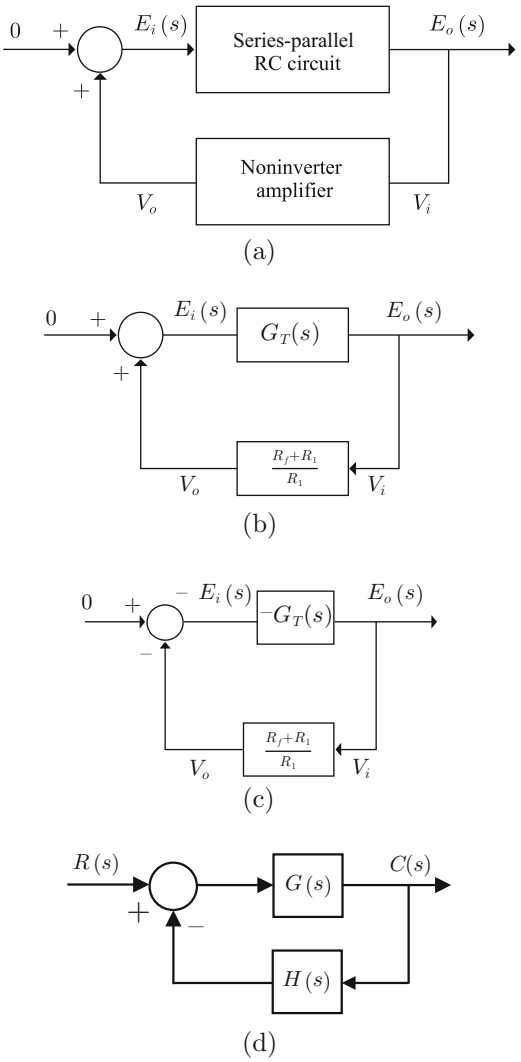

Fig. 9.18 Block diagrams equivalent to the circuit in Fig. 9.16

The closed-loop poles are the roots of this polynomial, i.e.,

$$s_1 = \frac{-(3-A)T + \sqrt{(3-A)^2T^2 - 4T^2}}{2T^2},$$

$$s_2 = \frac{-(3-A)T - \sqrt{(3-A)^2T^2 - 4T^2}}{2T^2}.$$

Note the following:

- Both poles have a nonzero imaginary part; hence, the circuit oscillates if:

$$(3-A)^2T^2 - 4T^2 < 0,$$

  i.e., if $5 > A > 1$.

- If $A > 3$, then both poles have a positive real part, i.e., the circuit is unstable, which is not desirable.
- If $A < 3$, then both poles have a negative real part, i.e., the circuit is stable. This, however, is not desirable either because circuit oscillation disappears as time increases.
- If $A = 3$, then both poles have a zero real part; thus, they are imaginary as desired. These poles are located at $s_{1,2} = \pm j\frac{1}{T}$. Hence, the oscillation frequency is $\omega = \frac{1}{T} = \frac{1}{RC}$.

9.3.3 *Frequency Response-Based Analysis*

Replace the variable change $s = j\omega$ in (9.5):

$$G_T(j\omega) = \frac{jT\omega}{T^2(j\omega)^2 + 3jT\omega + 1}.$$

Evaluating at the frequency $\omega = 1/T = 1/(RC)$:

$$G_T(j/T) = \frac{1}{3}.$$

To plot the Bode diagrams of $G_T(s)$ rearrange:

$$G_T(s) = Ts\frac{\frac{1}{T^2}}{s^2 + \frac{3}{T}s + \frac{1}{T^2}}. \tag{9.7}$$

The Bode diagrams of $G_T(s)$ are shown in Fig. 9.19. The magnitude of $G_T(j\omega)$ is maximal (equal to $\frac{1}{3}$) at the frequency $\omega = 1/T = 1/(RC)$, exactly when the phase of $G_T(j\omega)$ is zero.

The polar plot of $G(s)H(s)$, given in (9.6), is depicted in Fig. 9.20. From the Bode diagrams of $G_T(s)$, shown in Fig. 9.19, it is concluded that the polar plot of $G(s)H(s)$, shown in Fig. 9.20, consists of two clockwise contours. Note that the negative sign in (9.6) changes 180° the phase at every point of the Bode diagram of $G_T(s)$. Also note that the polar plot in Fig. 9.20 crosses the negative real axis at the point $-\frac{R_1+R_f}{3R_1}$ when the frequency is $\omega = 1/T = 1/(RC)$. On the other hand, because the polar plot includes positive and negative frequencies and it is symmetrical with respect to the real axis for negative and positive frequencies, then the negative real axis is also crossed at the point $-\frac{R_1+R_f}{3R_1}$ when the frequency is $\omega = -1/T = -1/(RC)$. Also note that the number of unstable open-loop poles of the function given in (9.6) is zero, i.e., $P = 0$, because all the coefficients of the polynomial at the denominator of $G_T(s)$ are positive (see Sect. 4.2.1).

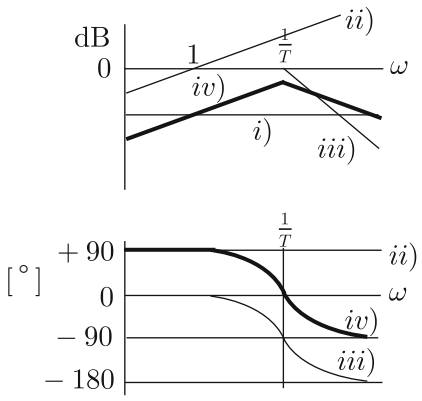

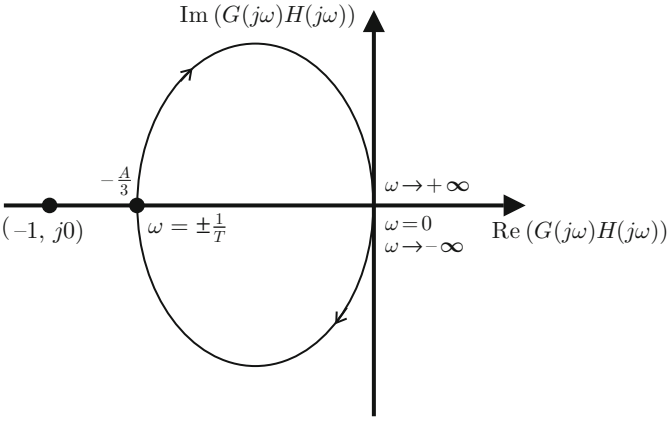

Fig. 9.19 Bode diagrams of $G_T(s)$ in (9.7). (i) T, (ii) s, (iii) $\frac{\frac{1}{T^2}}{s^2+\frac{3}{T}s+\frac{1}{T^2}}$, (iv) $G_T(s)$

Fig. 9.20 Polar plot of $G(s)H(s)$ in (9.6)

Finally, before applying the Nyquist stability criterion, the following must be noted. As $G(s)H(s)$ has one zero at $s = 0$, i.e., on the imaginary axis, a contour must be included such as that in Fig. 6.79. The only difference is that in this case it is a zero (instead of a pole) that must be contoured. However, along this contour $s = \varepsilon\angle\phi$ where $\varepsilon \to 0$; hence, $G(s)H(s) \to 0$ also on this contour. This means that $G(s)H(s)$ represents a unique point on the origin of the complete contour. Thus, when applying the Nyquist stability criterion, three cases exist:

1. If $\frac{R_1+R_f}{3R_1} > 1$, then the number of contours around the point $(-1, j0)$ is $N = 2$, i.e., the number of closed-loop unstable poles is $Z = N + P = 2$. This implies circuit instability, which is undesirable.
2. If $\frac{R_1+R_f}{3R_1} < 1$, then the number of contours around the point $(-1, j0)$ is $N = 0$ and the number of unstable closed-loop poles is $Z = N + P = 0$. Although this implies circuit stability, it is also undesirable in this application because the circuit oscillation disappears as time increases.

3. If $\frac{R_1+R_f}{3R_1} = 1$, then the circuit is marginally stable, i.e., there are closed-loop poles on the imaginary axis. This can also be understood as follows. The condition to be satisfied by the closed-loop poles is $1 + G(s)H(s) = 0$, or $G(s)H(s) = -1$. Then, if the closed-loop poles are imaginary, it suffices to perform the variable change $s = j\omega$. Note that this is what happens when the polar plot in Fig. 9.20 crosses the negative real axis at the point $(-1, j0)$ when the frequency is $\omega = 1/T = 1/(RC)$ and $\omega = -1/T = -1/(RC)$. This means that $G(j\omega)H(j\omega)|_{\omega=1/T} = -1$ and $G(j\omega)H(j\omega)|_{\omega=-1/T} = -1$. Hence, it is concluded that there are two closed-loop poles that are imaginary conjugate and placed at $s = j/T$ and $s = -j/T$. Thus, the circuit exhibits permanent oscillations at the frequency $\omega = 1/T$.

9.3.4 A Practical Oscillator

From the above discussion, it is concluded that the gain of the operational amplifier-based non-inverter amplifier must be chosen as:

$$A = \frac{R_1 + R_f}{R_1} = 3.$$

However, the circuit in Fig. 9.16 does not oscillate correctly. The reason for this is that commercial values for R_f and R_1 cannot be found to exactly satisfy $\frac{R_1+R_f}{R_1} = 3$. Moreover, any small change in their nominal values would render the circuit either unstable or stable (oscillation vanishes as time increases). This is a well-known fact in electronics: a linear circuit cannot correctly oscillate in practice, i.e., all practical oscillators are nonlinear.

The way to build a practical oscillator using the above ideas is by employing the circuit in Fig. 9.21, which includes a nonlinearity introduced by two Zener diodes. Suppose that $A > 3$. Hence, the circuit is unstable and oscillates with an ever increasing amplitude. The job of the Zener diodes is to put a short circuit at the 10[KOhm] resistance when they reach the avalanche voltage. This decreases the gain A of the amplifier when the output voltage reaches a certain threshold. This renders $A < 3$, and the oscillation amplitude decreases. Hence, the voltage at the Zener diodes decreases and the short circuit at the 10[KOhm] resistance disappears. Then, $A > 3$ again. Finally, this process ends at a steady state where a sinusoidal voltage with constant amplitude is produced. Note that, using the values of resistances in Fig. 9.21, $A = 45/10 = 4.5$ if the Zener diodes are open and $A = 35/10 = 3.5$ if the Zener diodes are on. Hence, the 25.6[KOhm] potentiometer must be adjusted to obtain a value slightly larger than 3 for A to obtain a sustained oscillation. Note that the expected oscillation frequency is:

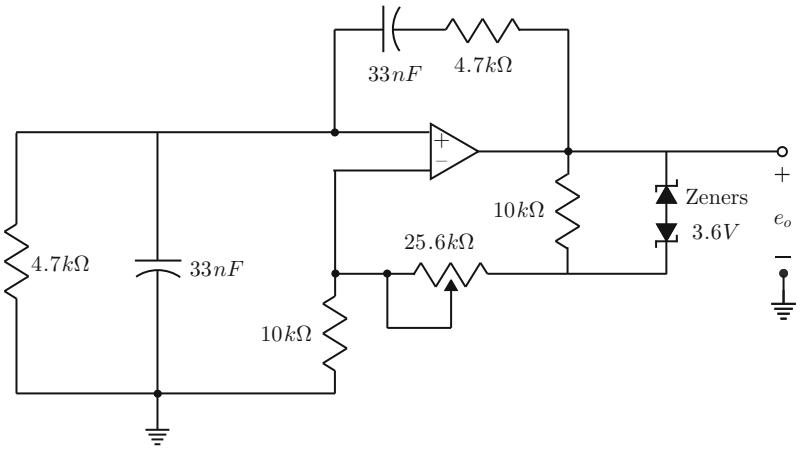

Fig. 9.21 Practical oscillator circuit

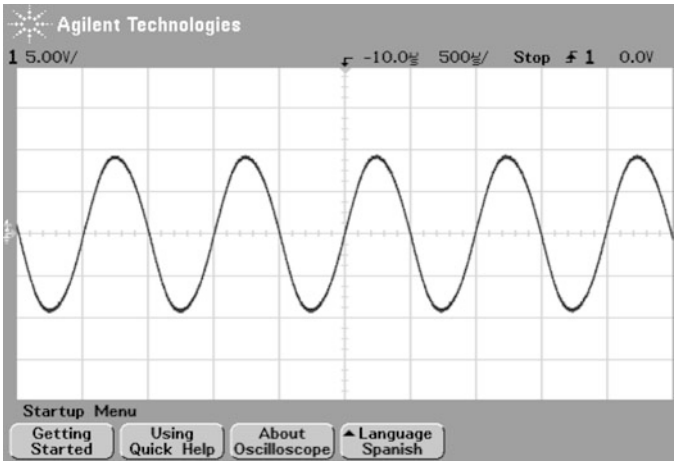

Fig. 9.22 Waveform of voltage at the output of the operational amplifier in Fig. 9.21. The potentiometer is at 20[KOhm]

$$\omega = \frac{1}{T} = \frac{1}{RC} = \frac{1}{(4.7 \times 10^3)(0.033 \times 10^{-6})} = 6447[\text{rad/s}],$$

$$f = \frac{\omega}{2\pi} = \frac{6447}{2\pi} = 1.026[\text{KHz}].$$

Some experimental results obtained with circuit in Fig. 9.21 are shown in Figs. 9.22 and 9.23. The UA741 operational amplifier has been employed. The frequency measured in experiments is 1[KHz]. The oscillation amplitude can be modified if the resistance of the 25.6[KOhm] potentiometer is increased, which also increases

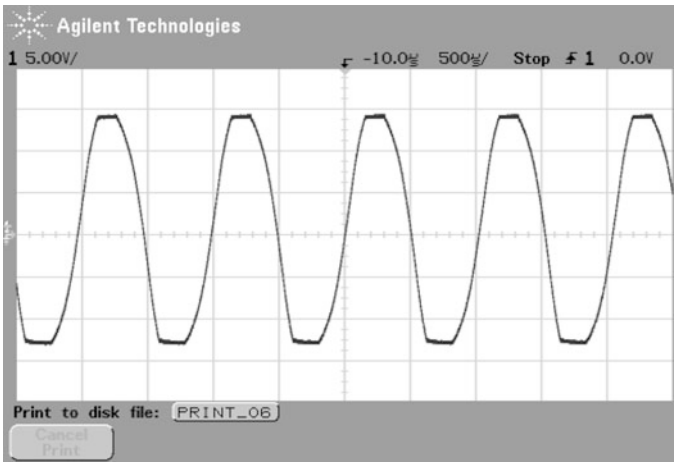

Fig. 9.23 Waveform of the voltage at the output of the operational amplifier in Fig. 9.21. The potentiometer is at 25.6[KOhm]

Fig. 9.24 Phase shift network

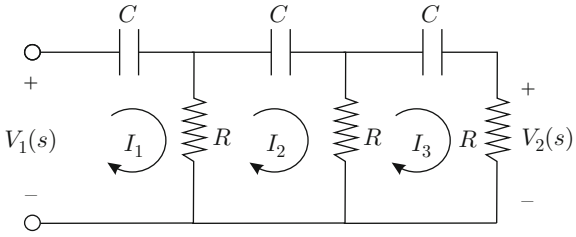

the amplifier gain A. However, if this gain is too large, the sinusoidal waveform is distorted. This is what happens in Fig. 9.23 where the 25.6[KOhm] potentiometer is adjusted to its maximal resistance value. On the contrary, in Fig. 9.22 the 25.6[KOhm] potentiometer is adjusted to approximately 20[KOhm]. This is evidence that the behavior of Zener diodes is smooth instead of abrupt, as the amplitude of voltage at the operational amplifier output increases. Thus, a larger loop gain in (9.6) reduces to 1 if the amplitude of oscillations increases, i.e., if the Zener diodes work deeper in the avalanche region.

Finally, note that, according to the block diagrams in Fig. 9.18, this oscillator circuit is a closed-loop system without an input, i.e., the circuit oscillates when a zero input is applied. This must not be a surprise as it is clearly explained in Sect. 3.3, Chap. 3, that a second-order (or a larger order) circuit may oscillate, despite the input being zero if the initial conditions are different from zero. In this respect, note that despite the fact that the circuit has no stored energy initially, some small initial conditions that are different from zero are produced as a consequence of a perturbation in the circuit when this is turned on. These initial conditions that are different from zero, although small, suffice to make the circuit oscillate given the initial instability of the circuit, because $A > 3$ when the circuit is turned on.

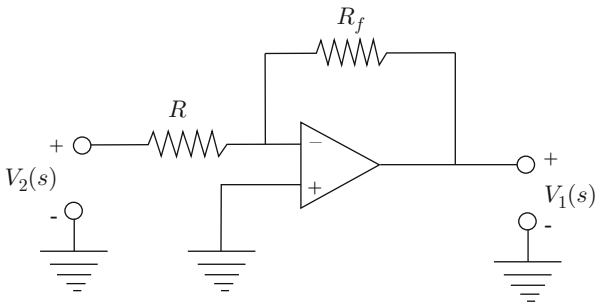

Fig. 9.25 Inverter amplifier

9.3.5 *Design Based on an Operational Amplifier: The Phase Shift Oscillator*

Consider the circuit shown in Fig. 9.24. The relationship between the voltages $V_1(s)$ and $V_2(s)$ is shown in (2.76) in Example 2.15, Chap. 2. This expression is rewritten here for ease of reference:

$$\frac{V_2(s)}{V_1(s)} = \frac{R^3C^3s^3}{R^3C^3s^3 + 6R^2C^2s^2 + 5RCs + 1} = F(s). \tag{9.8}$$

On the other hand, according to Sect. 9.2, the inverter amplifier shown in Fig. 9.25 performs the operation:

$$V_1(s) = -\frac{R_f}{R}V_2(s). \tag{9.9}$$

Now, consider the circuit shown in Fig. 9.26. Note that this circuit can be represented using the block diagram in Fig. 9.27a. Moreover, according to (9.8) and (9.9), the block diagram in Fig. 9.27b is obtained, which can be represented as in Fig. 9.27c. This is convenient for seeing that it is a negative feedback closed-loop system. Hence, the open-loop transfer function is given as:

$$G(s)H(s) = \frac{R_f}{R}F(s). \tag{9.10}$$

It is well known that the closed-loop poles satisfy:

$$1 + G(s)H(s) = 0, \tag{9.11}$$

i.e.,

$$1 + \frac{R_f}{R}F(s) = 0. \tag{9.12}$$

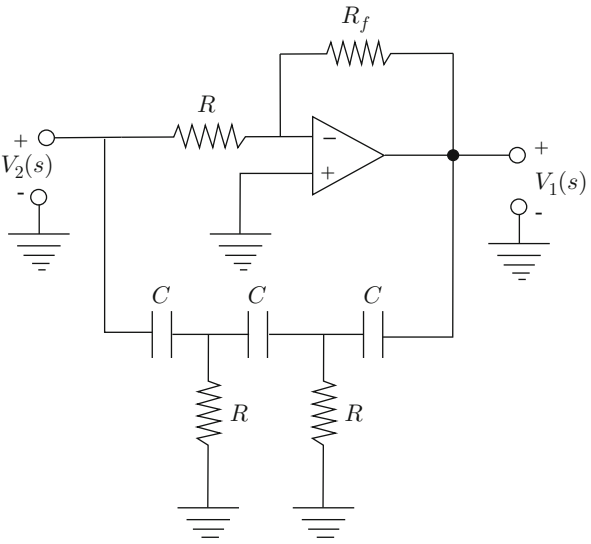

Fig. 9.26 Phase shift oscillator

Table 9.2 Applying Routh's criterion to the characteristic polynomial in (9.13)

s^3	$R^4C^3 + R_fR^3C^3$	$5R^2C$
s^2	$6R^3C^2$	R
s^1	$\frac{(6R^3C^2)(5R^2C)-R(R^4C^3+R_fR^3C^3)}{6R^3C^2}$	0
s^0	R	

9.3.6 Time Domain-Based Analysis

In the following, we analyze the closed-loop circuit to find the conditions for the existence of a pair of imaginary conjugate closed-loop poles. From (9.12), we obtain the following characteristic polynomial:

$$(R^4C^3 + R_fR^3C^3)s^3 + 6R^3C^2s^2 + 5R^2Cs + R = 0. \tag{9.13}$$

According to Chap. 3, the behavior of this circuit depends on the roots of the characteristic polynomial in (9.13). As this polynomial is third-degree, it is useful to employ Routh's stability criterion (Sect. 4.3) to study its roots; hence, Table 9.2 is obtained. Three different behaviors can be predicted from this table:

- $(6R^3C^2)(5R^2C) - R(R^4C^3 + R_fR^3C^3) > 0$, i.e., $R_f < 29R$. In this case, all the entries in the first column of Table 9.2 are positive, ensuring that all the roots of the polynomial in (9.13) have a negative real part, i.e., circuit stability is concluded. This means that, although the circuit could oscillate, this oscillation disappears as time increases.

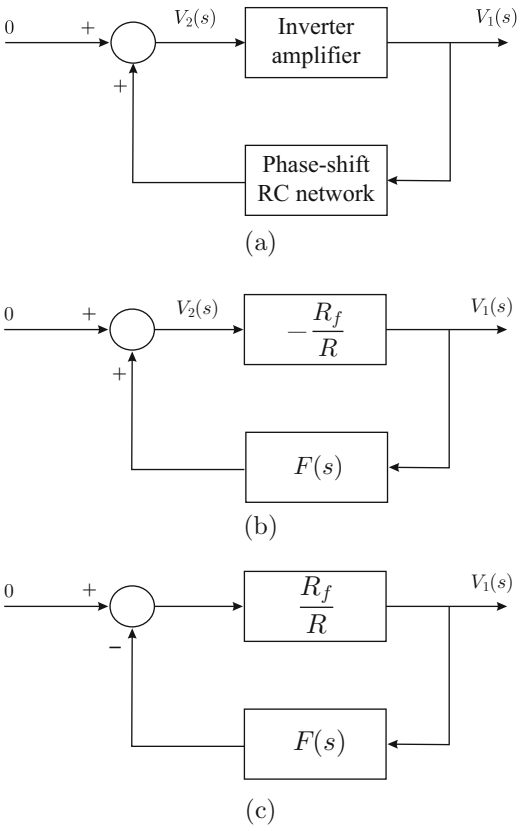

Fig. 9.27 Equivalent block diagrams for the circuit in Fig. 9.26

Table 9.3 Applying Routh's criterion to the characteristic polynomial in (9.13) (cont.)

s^3	$R^4C^3 + R_fR^3C^3$	$5R^2C$
s^2	$6R^3C^2$	R
s^1	$12R^3C^2$	0
s^0	R	

- $(6R^3C^2)(5R^2C) - R(R^4C^3 + R_fR^3C^3) < 0$, i.e., $R_f > 29R$. In this case, there are two changes of sign in the first column of Table 9.2. This means that the polynomial in (9.13) has two roots with a positive real part, i.e., circuit instability is concluded: although the circuit could oscillate, the amplitude of this oscillation would increase without a limit as time increases.
- $(6R^3C^2)(5R^2C) - R(R^4C^3 + R_fR^3C^3) = 0$, i.e., $R_f = 29R$. In this case, there is a row in Table 9.2 that is composed only of zeros (the row corresponding to s^1). In this case, Routh's criterion establishes (see Sect. 4.3, Example 4.14) that the derivative of the polynomial obtained from the row s^2 must be computed, i.e., $\frac{dP(s)}{ds} = 12R^3C^2s$, where $P(s) = 6R^3C^2s^2 + R$, to replace these coefficients in the row s^1 and to continue constructing the table as shown in Table 9.3. As there is no change of sign in the first column of Table 9.3, it is concluded that no roots

exist with positive real parts; hence, imaginary conjugate roots exist. Thus:

$$R_f = 29R, \tag{9.14}$$

is a necessary condition for circuit in Fig. 9.26 to exhibit sustained oscillations. To determine the oscillation frequency, it is useful to recall another property of data shown in Table 9.2 (see Sect. 4.3, Example 4.14): "if one row is composed only of zeros, then the roots of the polynomial obtained with data in the row immediately above the row composed of zeros are also roots of the characteristic polynomial in (9.13)". Hence, the roots of:

$$6R^3C^2s^2 + R = 0,$$

are also roots of the characteristic polynomial shown in (9.13). Solving the latter expression, it is found that the corresponding roots are imaginary, as expected:

$$s_1 = j\frac{1}{\sqrt{6}RC}, \quad s_2 = -j\frac{1}{\sqrt{6}RC}.$$

This means that $\omega = \frac{1}{\sqrt{6}RC} = 2\pi f$, i.e., that the oscillation frequency in Hertz is given as:

$$f = \frac{1}{2\pi\sqrt{6}RC}. \tag{9.15}$$

Thus, the oscillator circuit in Fig. 9.26 must be designed by choosing R and C such that the oscillation frequency is computed as in (9.15), and then oscillation is ensured by choosing R_f according to (9.14).

9.3.7 *Frequency Domain Analysis*

In what follows, the closed-loop circuit is studied by applying the Nyquist stability criterion to find the conditions for closed-loop marginal stability. Let us first apply Routh's criterion to the characteristic polynomial in (9.8) (see Table 9.4). As there are no changes of sign in the first column, we conclude that the characteristic

Table 9.4 Routh's criterion applied to the characteristic polynomial in (9.8)

s^3	R^3C^3	$5RC$
s^2	$6R^2C^2$	1
s^1	$\frac{29R^3C^3}{6R^2C^2}$	0
s^0	1	

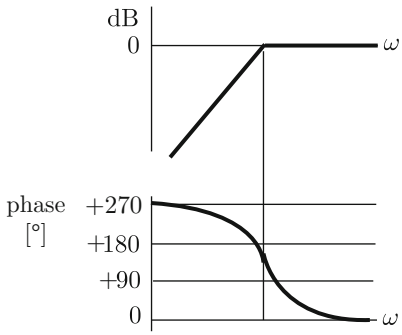

Fig. 9.28 Bode diagrams of $F(s)$ in (9.8)

polynomial in (9.8) has no pole with a positive real part. As $G(s)H(s) = \frac{R_f}{R}F(s)$, this means that $P = 0$. In Fig. 9.28, the Bode diagrams for $F(s)$ defined in (9.8) are depicted. From Fig. 9.28 the polar plot of $F(s)$ is obtained, which is depicted in Fig. 9.29. Note that, according to $G(s)H(s) = \frac{R_f}{R}F(s)$, the polar plot of the open-loop transfer function is identical to the polar plot of $F(s)$ in Fig. 9.29, but it is only required to increase the magnitude by a factor $\frac{R_f}{R}$. Hence, depending on the particular value of $\frac{R_f}{R}$, there are three possibilities, which are depicted in Fig. 9.30. Thus, closed-loop marginal stability is obtained for a value $\frac{R_f}{R}$ that satisfies $G(j\omega)H(j\omega) = -1$ for some ω. This means that the closed-loop poles are imaginary. Moreover, as $1 + G(s)H(s) = 0$ is the condition that defines the closed-loop poles s, then $1 + G(j\omega)H(j\omega) = 0$, or $G(j\omega)H(j\omega) = -1$, implies that the closed-loop poles can be written as $s = \pm j\omega$ where ω is the frequency at which the polar plot of $G(j\omega)H(j\omega)$ crosses the point $(-1, j0)$. The value of $\frac{R_f}{R}$ that produces marginal stability is known as the oscillation condition and can be obtained from $G(j\omega)H(j\omega) = \frac{R_f}{R}F(j\omega) = -1$, i.e.,

$$\frac{R_f}{R} = -\frac{1}{F(j\omega_2)}.$$

where ω_2 is the frequency when $\angle F(j\omega_2) = 180°$.

In Fig. 9.31, the Bode diagrams of $F(s)$ when $RC = 0.001$ are presented. These plots have been drawn using the following MATLAB code:

```
RC=0.001;
F=tf([RC^3 0 0 0],[RC^3 6*RC^2 5*RC 1]);
bode(F)
grid on
```

Note that $\angle F(j\omega_2) = 180°$ is obtained when $\omega_2 = 411$[rad/s] (the oscillation frequency) and $|F(j\omega_2)|_{[dB]} = -29.2$[dB]. Thus:

$$\frac{R_f}{R} = \frac{1}{10^{-29.2/20}} = 28.8403 \approx 29,$$

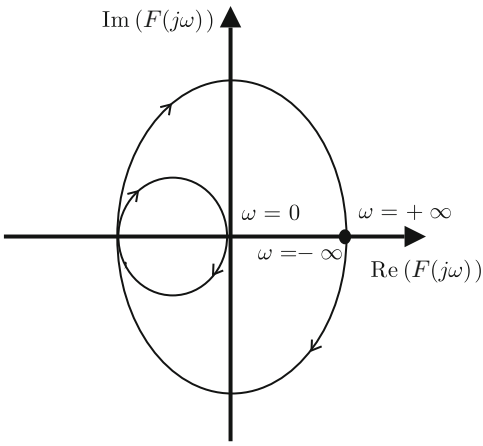

Fig. 9.29 Polar plot of $F(s)$ in (9.8)

a value that is very close to the oscillation condition established in (9.14). Also note that, according to the previous section, the oscillation frequency is given as $\omega = \frac{1}{\sqrt{6}RC} = 408.2483$[rad/s], where $RC = 0.001$ has been used, which is very close to $\omega_2 = 411$[rad/s] found in Fig. 9.31. Note that the frequency domain analysis does not provide closed expressions to compute the exact value of $\frac{R_f}{R}$ or the oscillation frequency. However, very precise numerical values are given for both parameters.

9.3.8 A Practical Oscillator Circuit

From the above discussion, it is concluded that R_f and R must satisfy (9.14). However, similar to the oscillator circuit in Sect. 9.3.1, the oscillator in Fig. 9.26 must be modified, as shown in Fig. 9.32 to accomplish a satisfactory oscillation. Note that, using the values of resistance in Fig. 9.32, $\frac{R_f}{R} = \frac{80000}{2200} = 36.36$ if the Zener diodes are open and $\frac{R_f}{R} = \frac{47000}{2200} = 21.36$ if the Zener diodes conduct. Hence, the 47[KOhm] potentiometer must be adjusted to obtain a value for $\frac{R_f}{R}$ slightly larger than 29 to obtain sustained oscillations. Note that the expected oscillation frequency is:

$$f = \frac{1}{2\pi\sqrt{6}RC} = \frac{1}{2\pi\sqrt{6}(2200)(0.01 \times 10^{-6})} = 2.9534[\text{KHz}].$$

Some experimental results are shown in Fig. 9.33 that were obtained with the circuit in Fig. 9.32. The UA741 operational amplifier is employed. Frequency measured in experiments is 2.7027[KHz], which is very close to the design value: 2.9534[KHz].

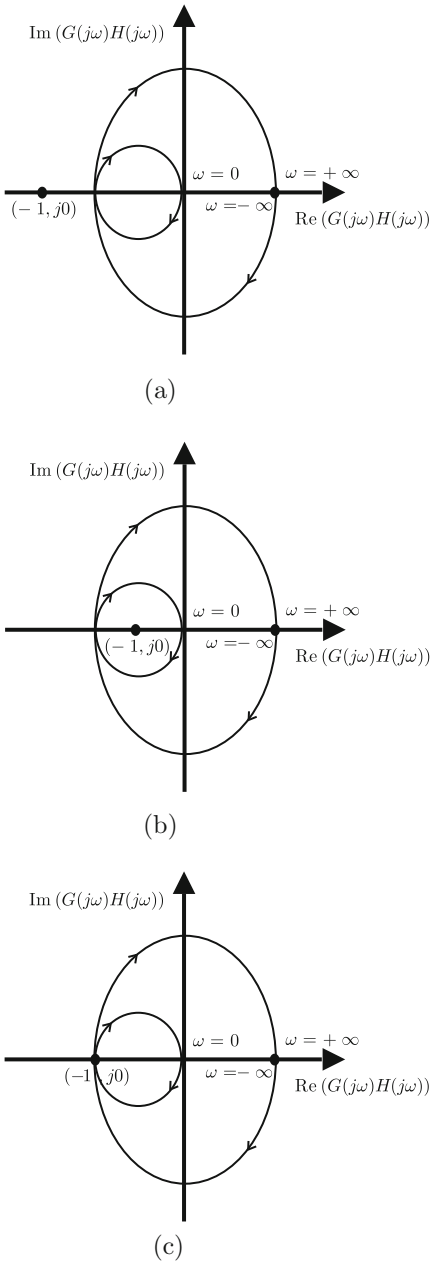

Fig. 9.30 Polar plots of $G(s)H(s)$ for different values of $\frac{R_f}{R}$. Recall that $P = 0$. (**a**) $N = 0$, $Z = N + P = 0$, closed-loop stability. (**b**) $N = 2$, $Z = N + P = 2$, closed-loop instability. (**c**) Closed-loop marginal stability

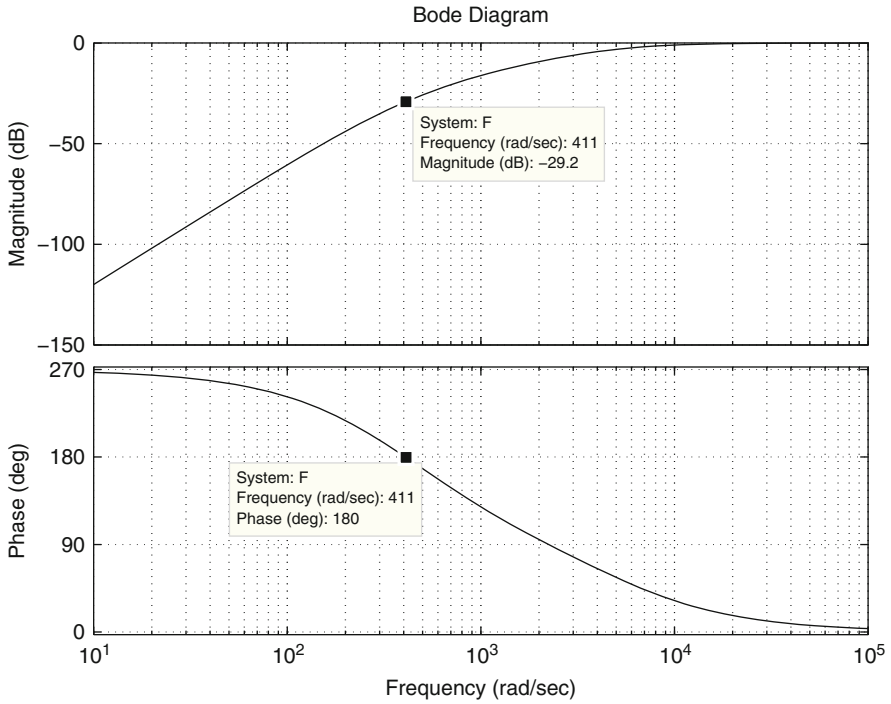

Fig. 9.31 Bode diagrams of $F(s)$ in (9.8), when $RC = 0.001$

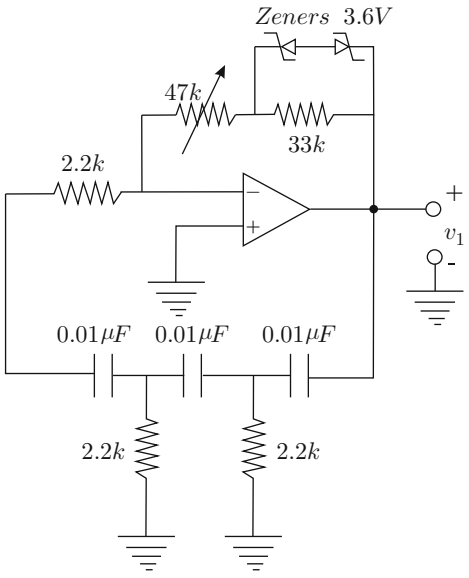

Fig. 9.32 A practical oscillator circuit

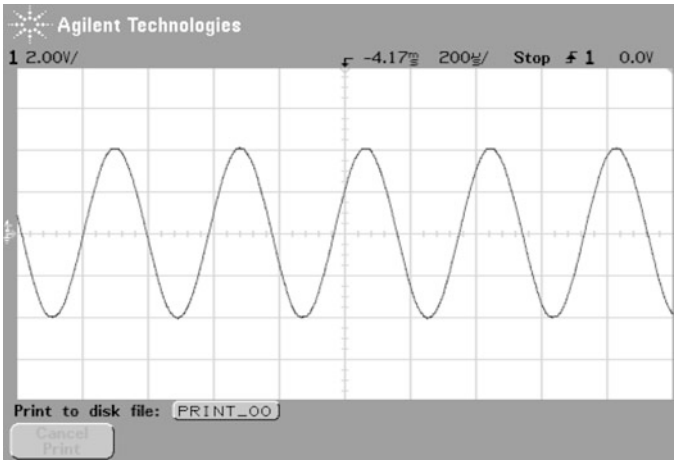

Fig. 9.33 Waveform of the voltage at the output of the operational amplifier in Fig. 9.32

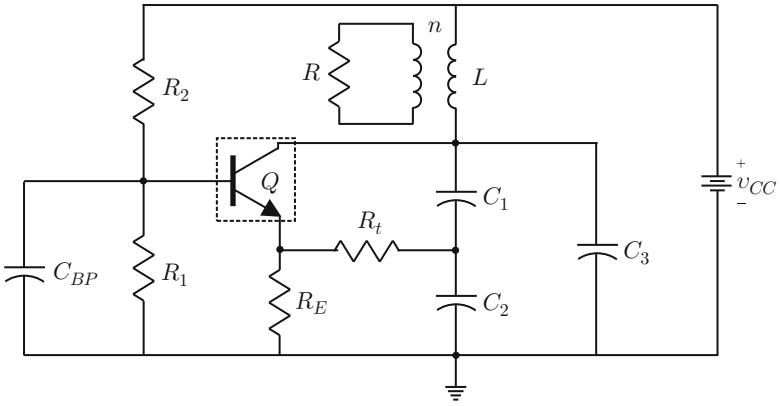

Fig. 9.34 Colpitts oscillator

9.3.9 A Transistor-Based Design

The oscillator circuit shown in Fig. 9.34 is studied in this section. This circuit is known as the Colpitts oscillator. The transistor is a nonlinear device. Because of that, the problem is studied by proceeding as in the case of nonlinear differential equations. It is assumed that the circuit in Fig. 9.34 works around an operation point, i.e., only small variations of signals are allowed around it. The operation point is determined by the direct current operation of the circuit in Fig. 9.34, whereas the variations around the operation point are analyzed using an equivalent small-signal circuit for the circuit in Fig. 9.34. The *small-signal circuit* is similar to approximate linear models obtained for nonlinear systems (nonlinear differential equations) in

Sect. 7.3, which is valid if only small variations around the selected operation point are allowed. The circuit is studied under direct current conditions in the next section. The equivalent small-signal circuit is analyzed in subsequent sections.

Given the large number of variables involved (voltages and currents at each circuit element), the following nomenclature is employed. v_{R1Q} stands for the (constant) voltage at the resistance R_1 at the operation point, v_{r1} represents the voltage variations at the resistance R_1 around the operation point and v_{R1} is the total voltage at the resistance R_1, i.e., $v_{R1} = v_{R1Q} + v_{r1}$. Currents and voltages at the other circuit elements are defined analogously. On the other hand, upper case letters are employed to represent the Laplace transform of a time function represented with a lower case letter, e.g., $I(s) = \mathcal{L}\{i(t)\}$.

9.3.10 Direct Current Analysis

The operation point in a transistor is determined by the constant values of the collector current i_{CQ} and the collector to emitter voltage v_{CEQ}. First, note that $v_{LQ} = L\frac{di_{LQ}}{dt} = 0, i_{C1Q} = C\frac{dv_{C1Q}}{dt} = 0, i_{C2Q} = C\frac{dv_{C2Q}}{dt} = 0$ e $i_{C3Q} = C\frac{dv_{C3Q}}{dt} = 0$ because i_{LQ}, v_{C1Q}, v_{C2Q} and v_{C3Q} are constants. Hence, the circuit in Fig. 9.35 is considered for the direct current analysis.

The fundamental direct current laws for a transistor establish that [1], Chap. 5:

$$i_{CQ} = \beta i_{BQ},\ i_{EQ} = (1+\beta)i_{BQ},\ \beta \gg 1,\ i_{EQ} \approx i_{CQ},\ v_{BEQ} = 0.7[\text{V}], \text{ silicon.}$$

The Kirchhoff voltage law applied to mesh defined by J_c in Fig. 9.35 yields:

$$\begin{aligned} v_{cc} &= v_{CEQ} + v_{REQ}, \\ v_{cc} &= v_{CEQ} + R_E i_{EQ}. \end{aligned} \tag{9.16}$$

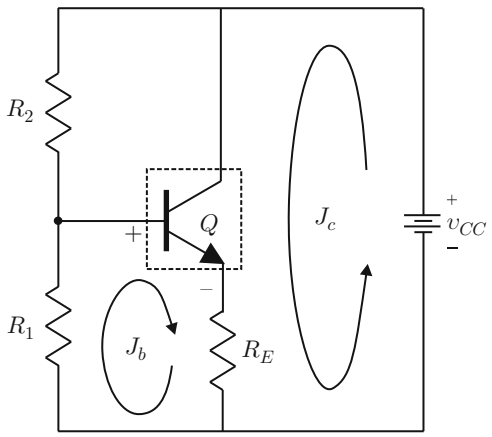

Fig. 9.35 Direct current equivalent circuit

The Kirchhoff voltage law applied to mesh defined by J_b in Fig. 9.35 yields:

$$v_{R1Q} = v_{BEQ} + v_{REQ}.$$
$$v_{R1Q} = 0.7 + R_E i_{EQ}. \tag{9.17}$$

Suppose that i_{CQ}, v_{CEQ}, β and v_{cc} are given as known values. R_E is computed using (9.16) and $i_{EQ} \approx I_{CQ}$. Then, i_{R1Q} is proposed from $i_{CQ} = \beta i_{BQ}$ and the following important assumption:

$$i_{R1Q} \gg i_{BQ}. \tag{9.18}$$

Hence, (9.17) can be employed to compute:

$$R_1 = \frac{v_{R1Q}}{i_{R1Q}}, \tag{9.19}$$

$$R_2 = \frac{v_{cc} - v_{R1Q}}{i_{R1Q}}. \tag{9.20}$$

The values for L, C_1, C_2, C_3, C_{BP} and R_t are computed from the analysis of the equivalent small-signal circuit, as shown in the following.

9.3.11 Equivalent Small-Signal Circuit

The equivalent small-signal model for the transistor is found first. Although several small-signal models for the transistor exist, in this book the following is considered. The emitter current, i.e., the current through the diode at the base-emitter junction, is given by the Shockley equation [1], chapter 5:

$$i_E = I_{ES}\left[e^{\frac{v_{BE}}{V_T}} - 1\right],$$

where I_{ES} is a constant with a value between 10^{-12}[A] and 10^{-16}[A] whereas $V_T = 0.026$[V] for a temperature of 300 Kelvin degrees. An important equation in the transistor establishes that $i_B = (1-\alpha)i_E$, where α is a positive constant slightly less than 1. Hence:

$$i_B = (1-\alpha)I_{ES}\left[e^{\frac{v_{BE}}{V_T}} - 1\right]. \tag{9.21}$$

As the transistor is assumed to work in its active region, then the number 1 subtraction in the latter expression can be neglected to write:

$$i_B = (1-\alpha)I_{ES}\left[e^{\frac{v_{BE}}{V_T}}\right].$$

Recalling that $i_B = i_{BQ} + i_b$ and $v_{BE} = v_{BEQ} + v_{be}$, the following can be written:

$$\begin{aligned} i_{BQ} + i_b &= (1-\alpha) I_{ES} \left[e^{\frac{v_{BEQ}+v_{be}}{V_T}} \right], \\ &= (1-\alpha) I_{ES} e^{\frac{v_{BEQ}}{V_T}} e^{\frac{v_{be}}{V_T}}. \end{aligned} \tag{9.22}$$

Also recall that small changes in i_B are due to small changes in v_{BE}, i.e., $i_b = 0$ if $v_{be} = 0$. Then, according to the last expression:

$$i_{BQ} = (1-\alpha) I_{ES} \left[e^{\frac{v_{BEQ}}{V_T}} \right].$$

Hence, (9.22) can be written as:

$$i_{BQ} + i_b = I_{BQ} e^{\frac{v_{be}}{V_T}}. \tag{9.23}$$

If only small values of v_{be} are allowed, the following approximation is possible [4], pp. 942:

$$e^{\frac{v_{be}}{V_T}} \approx 1 + \frac{v_{be}}{V_T},$$

which, together with (9.23), implies that:

$$i_b = \frac{v_{be}}{r_\pi}, \quad r_\pi = \frac{V_T}{I_{BQ}}. \tag{9.24}$$

On the other hand, the following expression is also valid for small variations:

$$i_c = \beta i_b. \tag{9.25}$$

Using (9.24) and (9.25) the small-signal model of the transistor shown in Fig. 9.36a is obtained. It is possible to find an equivalence between this model and that shown in Fig. 9.36b. Note that the only difference is that the base-emitter voltage is now given as a voltage drop due to the emitter current, i.e., it must depend on the new resistance h_{ib}:

$$v_{be} = h_{ib} i_e. \tag{9.26}$$

Comparing (9.24), (9.26), and using $i_e = (1+\beta) i_b$, the following is found:

$$h_{ib} = \frac{v_{be}}{i_e} = \frac{v_{be}}{(1+\beta) i_b} = \frac{r_\pi}{1+\beta} = \frac{V_T}{(1+\beta) I_{BQ}} = \frac{V_T}{I_{EQ}}. \tag{9.27}$$

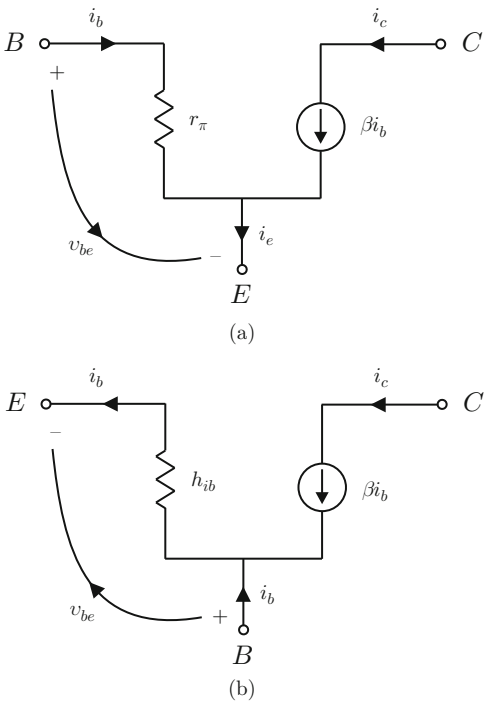

Fig. 9.36 Equivalent small-signal transistor models

Note that value of h_{ib} depends on I_{EQ}, i.e., on the operating point. Once the small-signal model of the transistor has been found, we proceed to finding the equivalent small-signal circuit for the whole oscillator circuit.

Consider the circuit in Fig. 9.37a. The Kirchhoff voltage law applied to mesh J_3 establishes that:

$$\begin{aligned} v_{cc} &= L\frac{di_L}{dt} + v_{CE} + v_{RE}, \\ i_L &= i_{LQ} + i_l, \\ v_{CE} &= v_{CEQ} + v_{ce}, \\ v_{RE} &= v_{REQ} + v_{re}. \end{aligned}$$

Suitably arranged, the latter expression can be written as:

$$v_{cc} = L\frac{d}{dt}(i_{LQ} + i_l) + v_{CEQ} + v_{ce} + v_{REQ} + v_{re}.$$

Using (9.16) and $v_{LQ} = L\frac{di_{LQ}}{dt} = 0$ in the previous expression, the following is found:

$$0 = L\frac{di_l}{dt} + v_{ce} + v_{re}.$$

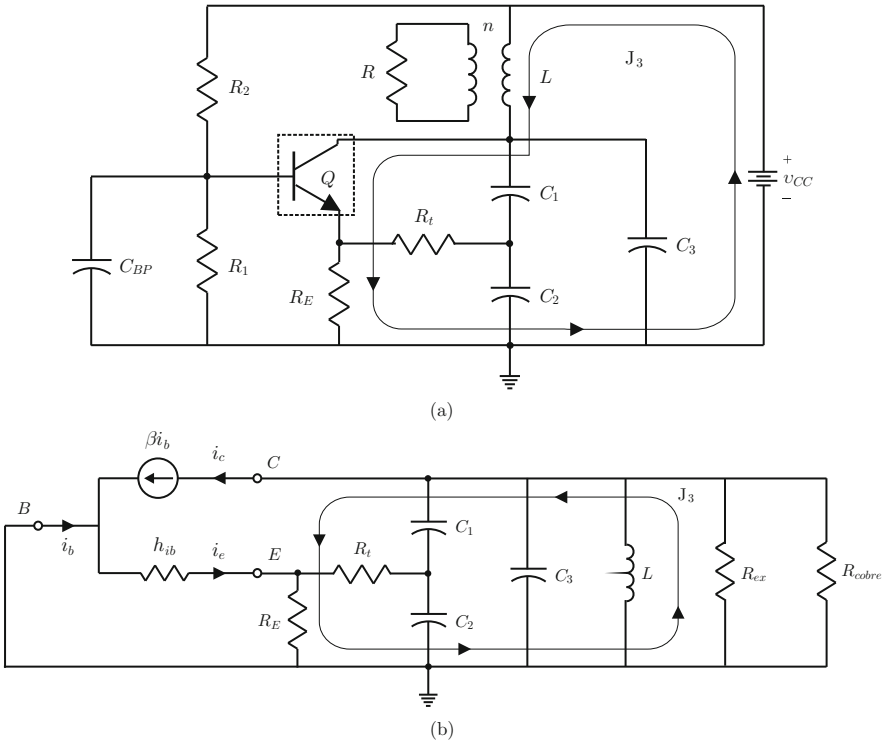

Fig. 9.37 Equivalent small-signal circuit for the whole oscillator circuit

Hence, the equivalent small-signal circuit must represent a mesh such as that indicated by J_3 in Fig. 9.37b. Proceeding in a similar manner for all possible meshes and nodes in the circuit depicted in Fig. 9.37a, it is found that the equivalent small-signal circuit is given as in Fig. 9.37b. It is important to state that R_{copper} is the equivalent parallel resistance of the inductance internal resistance (due to copper), whereas $R_{ex} = n^2 R$, where R is the external load for the oscillator circuit and n is the ratio of the turns number of L and the turns number of the inductance connected to R.

Finally, the resistances R_1 and R_2 in Fig. 9.37a disappear in Fig. 9.37b because it is assumed that the impedance of C_{BP} (parallel to R_1 and R_2) is very small compared with the equivalent parallel resistance of R_1 and R_2 at the oscillation frequency ω_1, i.e., $\frac{1}{\omega_1 C_{BP}} \ll \frac{R_1 R_2}{R_1 + R_2}$. Moreover, if $\frac{1}{\omega_1 C_{BP}} \ll h_{ib}$, the capacitor impedance can be neglected.

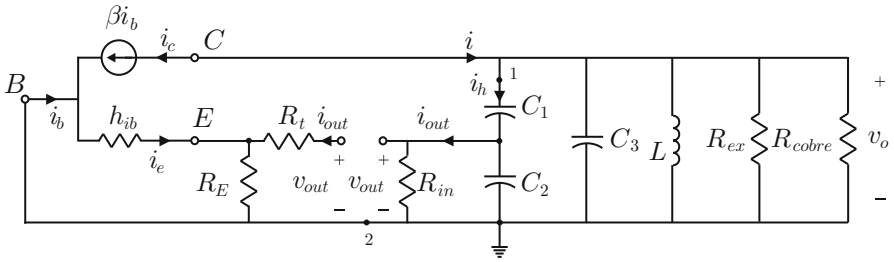

Fig. 9.38 Circuit employed for analysis purposes

9.3.12 Closed-Loop System Equations

The circuit in Fig. 9.34 is analyzed in this and the subsequent sections on the basis of the equivalent small-signal circuit in Fig. 9.37b. The reader must remember that all that is predicted by this analysis only stands around the operation point, which is determined in the direct current analysis.

For analysis purposes, the feedback path through the emitter resistance is opened as shown in Fig. 9.38 [5], pp. 265, [6], pp. 64. R_{in} in Fig. 9.38 is given as:

$$R_{in} = R_t + \frac{R_E h_{ib}}{R_E + h_{ib}}. \tag{9.28}$$

Now, we proceed to analyze the circuit in Fig. 9.38. The impedance between points 1 and 2 is given as:

$$Z_f(s) = \frac{1}{Y_f(s)} = \frac{1}{sC_1} + \frac{R_{in}\frac{1}{sC_2}}{R_{in} + \frac{1}{sC_2}} = \frac{sR_{in}(C_1 + C_2) + 1}{sC_1(sC_2R_{in} + 1)}, \tag{9.29}$$

where $Y_f(s)$ is the admittance between points 1 and 2. On the other hand, $V_o(s)$ and $I(s)$ are related as:

$$V_o(s) = Z_c(s)I(s), \tag{9.30}$$

where:

$$\frac{1}{Z_c(s)} = Y_f(s) + \frac{1}{sL} + sC_3 + \frac{1}{R_{ex}} + \frac{1}{R_{copper}}. \tag{9.31}$$

After an algebraic procedure, it is found that:

$$Z_c(s) = \frac{sL(sR_{in}(C_1 + C_2) + 1)}{a_3s^3 + a_2s^2 + a_1s + 1}, \tag{9.32}$$

$$a_3 = L(C_1C_2 + C_3(C_1 + C_2))R_{in},$$
$$a_2 = LC_1 + LC_3 + \frac{R_{copper} + R_{ex}}{R_{copper}R_{ex}}LR_{in}(C_1 + C_2),$$
$$a_1 = R_{in}(C_1 + C_2) + \frac{R_{copper} + R_{ex}}{R_{copper}R_{ex}}L.$$

Voltage $V_{out}(s)$ can be computed as:

$$V_{out}(s) = M(s)V_o(s), \tag{9.33}$$

where $V_{out}(s)$ and $V_o(s)$ are related to current $I_h(s)$ through:

$$V_o(s) = \frac{1}{Y_f(s)}I_h(s), \quad V_{out}(s) = \frac{1}{\frac{1}{R_{in}} + sC_2}I_h(s). \tag{9.34}$$

Combining both expressions in (9.34), the following is found:

$$V_o(s) = \frac{1}{Y_f(s)}\frac{1 + R_{in}sC_2}{R_{in}}V_{out}(s).$$

Use of (9.29) yields:

$$M(s) = \frac{V_{out}(s)}{V_o(s)} = \frac{s(R_{in}^2C_1C_2s + R_{in}C_1)}{R_{in}^2C_2(C_1 + C_2)s^2 + R_{in}(2C_2 + C_1)s + 1}. \tag{9.35}$$

According to (9.33) and (9.30), the following is found:

$$I_{out}(s) = \frac{V_{out}(s)}{R_{in}} = \frac{1}{R_{in}}M(s)V_o(s) = \frac{1}{R_{in}}M(s)Z_c(s)I(s). \tag{9.36}$$

On the other hand, applying the current divisor to the emitter circuit in Fig. 9.38, the following is found:

$$I_e(s) = \frac{-R_E}{R_E + h_{ib}}I_{out}(s).$$

Thus, if:

$$R_E \gg h_{ib}, \quad \beta \gg 1, \tag{9.37}$$

then it can be approximated:

$$I_{out}(s) \approx -I_e(s) = -(\beta + 1)I_b(s) \approx -\beta I_b(s) = I(s), \tag{9.38}$$

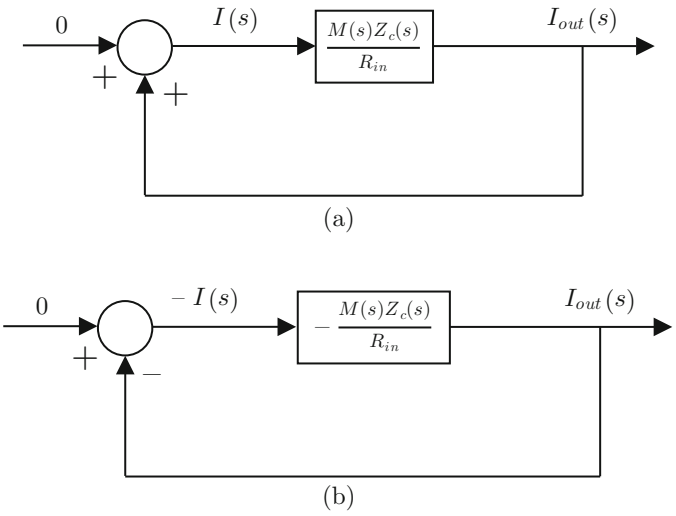

Fig. 9.39 Equivalent block diagrams for the circuit in Fig. 9.38

i.e., the transistor current gain in the common base configuration is unitary. According to the expressions in (9.36) and (9.38), the block diagram in Fig. 9.39a is obtained. This block diagram has positive feedback, which is an important feature for producing sustained oscillations. In Fig. 9.39b an equivalent block diagram is shown, which, however, is now expressed as a negative feedback system. This allows the application of classical control analysis and design tools when applied to a closed-loop system such as that in Fig. 9.18d. Hence, the open-loop transfer function is:

$$G(s)H(s) = -\frac{1}{R_{in}} M(s)Z_c(s). \tag{9.39}$$

9.3.13 *Conditions for Ensuring Sustained Oscillations*

Let us first study the transfer functions $M(s)$ and $Z_c(s)$. Note that all the coefficients of these transfer functions are positive. According to the criteria studied in Sects. 4.2.1 and 4.2.2 on the coefficient signs of first- and second-order polynomials and their corresponding roots, it is concluded that $M(s)$ has two poles with a negative real part, one zero with a negative real part and one zero at $s = 0$.

However, according to Sect. 4.2.3, the coefficient signs criterion cannot be applied to $Z_c(s)$ because its denominator is a third-degree polynomial. Nevertheless, a well-known result of the linear electric circuit theory[1] can be employed. This result

[1] Routh's criterion can also be used, if preferred.

states [7], Chapt. 19, Sects. 5 and 6, that the impedance of any network composed only of passive circuit elements (resistances, capacitance, and inductances) is a transfer function that only has poles with real parts, which are less than or equal to zero. Note that this is the case of $Z_c(s)$. Furthermore, as $Z_c(s)$ has a denominator with a term that is independent of s, then it is ensured that $Z_c(s)$ has three poles with a negative real part, one zero with a negative real part, and one zero at $s = 0$.

According to the above discussion and what was presented in Chap. 6, it is concluded that the Bode and polar plots of $Z_c(s)$ and $M(s)$ have the shapes shown in Figs. 9.40 and 9.41 respectively, whereas the polar plot of $G(s)H(s)$ given in (9.39) is shown in Fig. 9.42. It is important to stress that the polar plot of $G(s)H(s)$ is composed of two clockwise closed contours obtained as the frequency goes from $-\infty$ to $+\infty$. The real axis is crossed twice at the frequencies $\omega = \pm\omega_1$. Note that, at these frequencies, the transfer function $G(j\omega)H(j\omega)$ has a zero imaginary part. Finally, as $G(s)H(s)$ has two zeros at $s = 0$, to apply the Nyquist criterion the contour shown in Fig. 6.79 must be performed around such zeros at origin. However, as $s = \varepsilon\angle\phi$, with $\varepsilon \to 0$, then $G(s)H(s) \to 0$ along the complete contour; hence, it is represented by a single point at the origin. Applying the Nyquist criterion, the following conclusions are in order:

- If $|G(j\omega)H(j\omega)|_{\omega=w_1} < 1$, then closed-loop stability is ensured and sustained oscillations are not possible. This is because $Z = P+N$, where $P = 0$ represents the number of poles with positive real parts in $G(s)H(s)$, $N = 0$ is the number of clockwise contours around the point $(-1, 0)$ in Fig. 9.42 and $Z = 0$ is the number of closed-loop unstable poles.
- If $|G(j\omega)H(j\omega)|_{\omega=w_1} > 1$, then the closed-loop system is unstable because $Z = N + P = 2$, with $P = 0$ and $N = 2$. This situation is clearly undesirable.
- If $|G(j\omega)H(j\omega)|_{\omega=w_1} = 1$, then there are two imaginary closed-loop poles that allows the existence of sustained oscillations. The imaginary part of these poles is $\pm\omega_1$ representing the circuit oscillation frequency.

From these observations, a way of computing the values for the circuit elements is presented next. However, given the complexity of the expressions defining $G(s)H(s)$, some assumptions about the circuit components must be considered.

9.3.14 Computing the Circuit Components

First, compute the following expression:

$$\frac{1}{Z_c(j\omega)} = \frac{\omega^2 C_1^2 R_{in}}{(\omega R_{in}(C_1 + C_2))^2 + 1} + \frac{1}{R_{ex}} + \frac{1}{R_{copper}} + j\left[\omega C_1 \frac{\omega^2 C_2 R_{in}^2 (C_1 + C_2) + 1}{(\omega R_{in}(C_1 + C_2))^2 + 1} + \omega C_3 - \frac{1}{\omega L}\right], \tag{9.40}$$

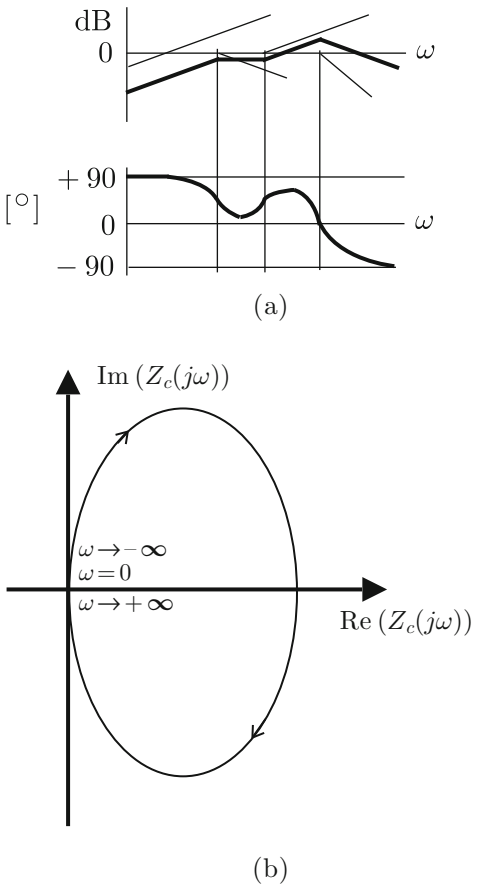

Fig. 9.40 Frequency response plots for $Z_c(s)$ in (9.32) . (**a**) Bode diagrams of $Z_c(s)$. (**b**) Polar plot of $Z_c(s)$ (two turns)

by performing the variable change $s = j\omega$ in (9.31), and the following expression:

$$M(j\omega) = \frac{R_{in}^2\omega^2(C_1^2 + C_1C_2) + j\omega R_{in}C_1}{1 + R_{in}^2\omega^2(C_1 + C_2)^2}. \tag{9.41}$$

by performing the variable change $s = j\omega$ in (9.35). To render the procedure for obtaining this expression easier, it is important to state that, during such a procedure, the factor $1 + R_{in}^2\omega^2C_2^2$ appears at both the numerator and the denominator of $M(j\omega)$; hence, they cancel each other out to finally obtain (9.41).

As previously observed, the polar plot of $G(j\omega)H(j\omega)$ crosses the negative real axis at the frequency ω_1. This means that the imaginary part of (9.40) and (9.41) must be zero when evaluated at $\omega = \omega_1$. Applying this condition in (9.40), the following is found:

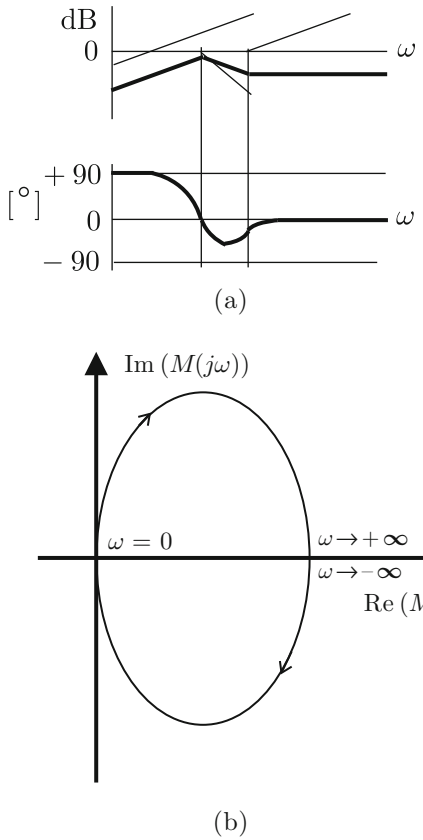

Fig. 9.41 Frequency response plots for $M(s)$ in (9.35) . (**a**) Bode diagrams of $M(s)$. (**b**) Polar plot of $M(s)$

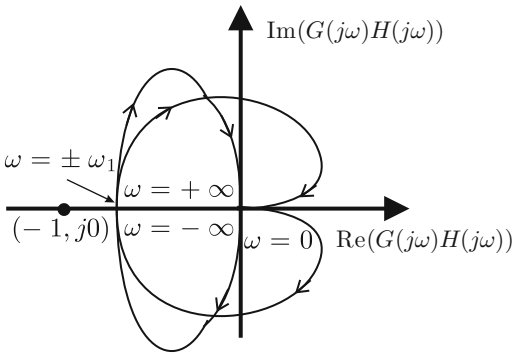

Fig. 9.42 Polar plot of $G(s)H(s)$ in (9.39)

$$\omega_1 = \frac{1}{\sqrt{L\left[\frac{C_1C_2}{C_1+C_2} + C_3\right]}}, \tag{9.42}$$

, which represents the circuit oscillation frequency. It is very important to state that, to simplify these expressions to obtain (9.42), the following assumptions have to be considered:

$$R_{in}^2 \gg \frac{1}{\omega_1^2 C_2(C_1+C_2)}, \quad R_{in}^2 \gg \frac{1}{\omega_1^2 (C_1+C_2)^2}. \tag{9.43}$$

On the other hand, the phase of (9.41) is given as:

$$\angle M(j\omega) = \arctan\left(\frac{\frac{1}{\omega(C_1+C_2)}}{R_{in}}\right). \tag{9.44}$$

Note that this phase is different from zero for any frequency. The above-cited condition requiring the imaginary part of $M(j\omega)$ to be zero is equivalent to asking for the phase in (9.44) to be zero. Although this is not possible, a phase that is close to zero can be obtained for $\omega = \omega_1$ if:

$$R_{in} \gg \frac{1}{\omega_1(C_1+C_2)}. \tag{9.45}$$

This and the other approximations that have been considered result in only small differences between the computed values and those obtained experimentally on the oscillation frequency and the gain of the open-loop transfer function.

Finally, $G(j\omega)H(j\omega)|_{\omega=w_1}$ is obtained as:

$$|G(j\omega)H(j\omega)|_{\omega=w_1} = \frac{1}{R_{in}} \mathrm{Re}(M(j\omega))|_{\omega=\omega_1} \mathrm{Re}(Z_c(j\omega))|_{\omega=\omega_1}, \tag{9.46}$$

where $\mathrm{Re}(x)$ stands for the real part of x. From (9.46) and taking into account the assumption in (9.45), the following is found:

$$|G(j\omega)H(j\omega)|_{\omega=w_1} = \frac{1}{R_{in}\frac{C_1+C_2}{C_1}} \left[\frac{1}{\frac{C_1^2}{R_{in}(C_1+C_2)^2} + \frac{1}{R_{ex}} + \frac{1}{R_{copper}}}\right].$$

Hence, according to the condition $|G(j\omega)H(j\omega)|_{\omega=w_1} = 1$, it is concluded that the circuit presents sustained oscillations at the frequency given in (9.42) if:

$$\frac{1}{R_{in}\frac{C_1+C_2}{C_1}} \left[\frac{1}{\frac{C_1^2}{R_{in}(C_1+C_2)^2} + \frac{1}{R_{ex}} + \frac{1}{R_{copper}}}\right] = 1. \tag{9.47}$$

Similar to the case of an oscillator based on an operation amplifier, it is important to stress the following. It is not possible to satisfy the condition (9.47) in practice

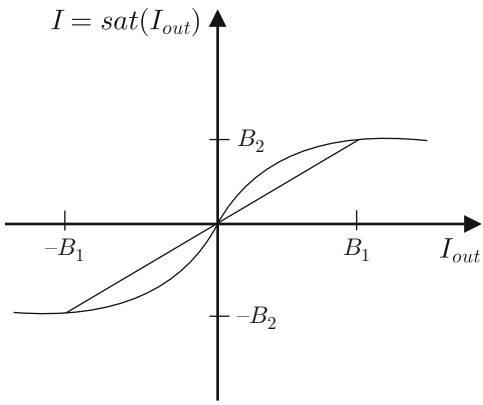

Fig. 9.43 Real characteristic between the emitter current and the collector current in a transistor

because of the uncertainties present in the commercial values of the components involved in such a condition. Furthermore, these parameters may present changes during normal circuit operation. The way of solving this problem in practice is to use the following condition instead of (9.47):

$$\frac{1}{R_{in}\frac{C_1+C_2}{C_1}}\left[\frac{1}{\frac{C_1^2}{R_{in}(C_1+C_2)^2}+\frac{1}{R_{ex}}+\frac{1}{R_{copper}}}\right] > 1. \tag{9.48}$$

This renders the circuit unstable when turned on and, because of that, the amplitude of the oscillation increases. However, this amplitude growth does not stand forever because the transistor reaches saturation (zero collector to emitter voltage and maximal collector current) and cutoff (zero collector current and maximal collector to emitter voltage) regions. Hence, I_{out} and I in Fig. 9.39b are related through a saturation function as $I = sat(I_{out})$ shown in Fig. 9.43. The transistor current gain corresponds to the slope $\frac{B_2}{B_1}$, where B_1 is the amplitude of I_{out} and B_2 is the amplitude of I. Then, the block diagram in Fig. 9.39b must be changed by that in Fig. 9.44 and we now have:

$$G(j\omega)H(j\omega)|_{\omega=w_1} = \frac{B_2}{B_1}\frac{1}{R_{in}\frac{C_1+C_2}{C_1}}\left[\frac{1}{\frac{C_1^2}{R_{in}(C_1+C_2)^2}+\frac{1}{R_{ex}}+\frac{1}{R_{copper}}}\right]. \tag{9.49}$$

Note that the slope $\frac{B_2}{B_1}$ is equal to 1 for the amplitudes of I_{out}, i.e., B_1, which are close to zero, but $\frac{B_2}{B_1}$ decreases to zero as B_1 grows. Hence, if (9.48) is satisfied, there always exists an oscillation amplitude such that (9.49) becomes 1 and the desired sustained oscillations are obtained. Although this suggests that the left hand

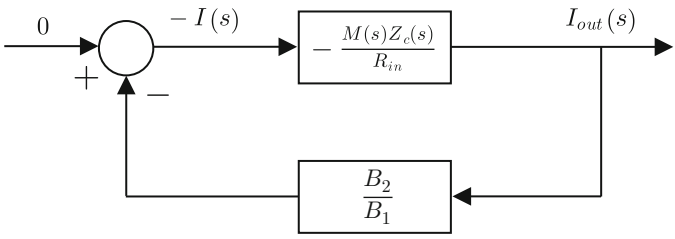

Fig. 9.44 Block diagram considering saturation in the collector current

in (9.48) can be designed to be as large as desired, this is not recommended and a value close to 1 must be designed. The reason for this is that large values for the left-hand side of (9.48) require a strong reduction in the current gain, which implies that the transistor works deep in its nonlinear region, i.e., the sinusoidal waveform is strongly distorted.

Another more formal way of explaining the sustained oscillations in this oscillator circuit is based on the limit cycle analysis presented in Sects. 8.3.3 and 8.3.4. According to Fig. 9.42, the polar plot of $G(s)H((s)$ crosses the negative real axis in the open interval $(-\infty, -1]$, if closed-loop instability is designed, i.e., as desired in an oscillator circuit. On the other hand, according to Sect. 8.3.3, the plot of $-1/N(A)$, where $N(A)$ is the describing function of transistor saturation, is represented by the open real interval $(-\infty, -1]$ in Fig. 9.42. According to Sects. 8.3.3 and 8.3.4, these conditions suffice for a stable limit cycle to appear. This means that sustained oscillations appear instead of closed-loop instability. Moreover, if the left-hand side of (9.48) is larger, then the point where $G(j\omega)H(j\omega)$ crosses the real open interval $(-\infty, -1]$ moves to the left, which, according to Sects. 8.3.3 and 8.3.4, implies that a larger oscillation amplitude of the limit cycle is produced. This, however, results in a more distorted waveform because of the saturation nonlinearity.

On the other hand, note that the conditions (9.43), (9.45) are immediately satisfied if:

$$R_{in} \gg \frac{1}{\omega_1 C_2}. \tag{9.50}$$

The conditions (9.37) and (9.50) are important for design purposes as explained in the following. The first of these conditions ensures that the current gain of the common base configuration is unitary, whereas the second one ensures that the capacitor C_2 is not put into the short circuit by the resistance R_{in}. If this were the case, the feedback through the capacitive network composed of C_1 and C_2 would not work correctly. Also note that the expression between brackets in (9.48) stands for the parallel equivalent resistance of R_{ex}, R_{copper} and R_{in} multiplied by the constant factor $[(C_1 + C_2)/C_1]^2$. R_{in} is commonly small compared with R_{ex} and R_{copper}. If the factor $(C_1 + C_2)/C_1$ is chosen to be large through:

$$C_2 \geq 10C_1, \tag{9.51}$$

then it is ensured that the value of the factor between brackets in (9.48) is approximately the equivalent parallel resistance of R_{ex} and R_{copper}. Hence, the left hand in (9.48) is given by this equivalent parallel resistance (which is large compared with R_{in}) divided by the factor $R_{in}(C_1 + C_2)/C_1$. This ratio can be rendered slightly larger than 1 if (9.51) is used. Thus, the design rules for the oscillator are summarized by (9.37), (9.50), (9.51), (9.42), and (9.48). It is interesting to state that these conditions appear in the books concerned with the electronic design of this class of oscillator [6], pp. 65, [8], pp. 9–13.

Finally, note the advantages of the frequency response techniques with respect to the time response techniques (based on the location of the closed-loop system poles) in this problem. When trying to apply the latter of these methods, a fifth-order characteristic polynomial is found. When trying to use Routh's criterion to establish the conditions to obtain imaginary closed-loop poles, a complex problem is found: the resulting conditions are expressed in a very complex manner and it is difficult to find clear design rules such as those in (9.37), (9.42), (9.48), (9.50), (9.51).

9.3.15 *Experimental Results*

In this section, an oscillator circuit is designed and experimentally tested to generate a sinusoidal waveform at 1.8[MHz]. The design data are the following. $v_{CC} = 12$[V], $i_{EQ} \approx i_{CQ} = 1.3$[mA], $v_{CEQ} = 10.7$[V].

A PN2222A transistor is selected that has $\beta = 200$. Using (9.16), the following is found:

$$R_E = 1[\text{KOhm}].$$

From $i_{CQ} = \beta i_{BQ}$ it is found that $i_{BQ} = 6.5 \times 10^{-3}$[mA]. According to (9.18), $i_{R1Q} = 1$[mA] is proposed. With this and (9.17), (9.19), (9.20), the following is computed:

$$R_1 = 2[\text{KOhm}], \quad R_2 = 10[\text{KOhm}].$$

The inductance is $L = 0.328 \times 10^{-3}$[Hy], with an equivalent parallel internal resistance $R_{copper} = 101677$[Ohm]. Capacitances $C_1 = 27 \times 10^{-12}$[F], $C_2 = 200 \times 10^{-12}$[F] are employed and it is assumed that the capacitor C_3 is not present, i.e., $C_3 = 0$. Note that this selection of capacitors approximately satisfies (9.51). Hence, using (9.42), it is found that the circuit oscillation frequency is $f_1 = 1.8018$[MHz], i.e., $\omega_1 = 2\pi f_1 = 1.132 \times 10^7$[rad/s].

On the other hand, it is also assumed that the oscillator has no external load i.e., $R_{ex} \to \infty$ or $1/R_{ex} = 0$. Using $R_t = 10000$[Ohm], $V_T = 0.026$[V], $i_{EQ} = 1.3$[mA], (9.27), and (9.28), $R_{in} = 10020$[Ohm] is found. With these data, the following is found:

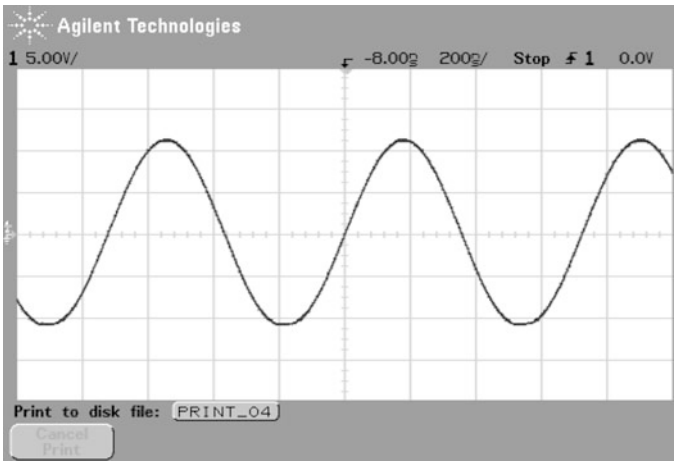

Fig. 9.45 Voltage waveform at the inductance terminals when $R_t = 10000$[Ohm]

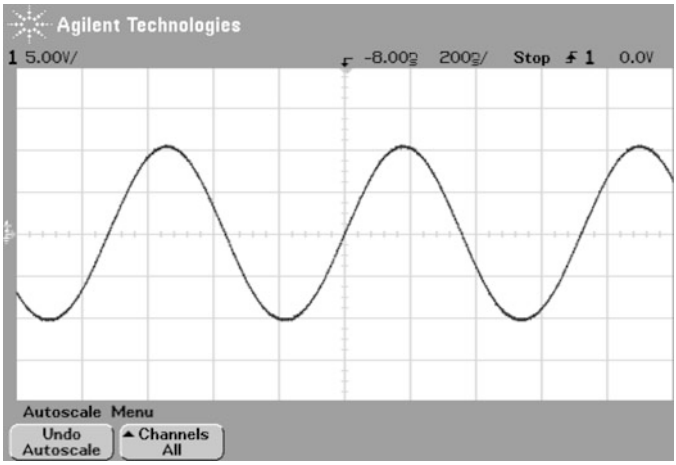

Fig. 9.46 Voltage waveform at the inductance terminals when $R_t = 11000$[Ohm]

$$\frac{1}{R_{in}\frac{C_1+C_2}{C_1}}\left[\frac{1}{\frac{C_1^2}{R_{in}(C_1+C_2)^2}+\frac{1}{R_{ex}}+\frac{1}{R_{copper}}}\right]=1.1363,$$

i.e., (9.48), (9.50), (9.37), are satisfied. On the other hand, $C_{BP} = 0.1 \times 10^{-6}$[F] is used and $\frac{1}{\omega_1 C_{BP}} = 0.883$[Ohm]$\ll \frac{R_1 R_2}{R_1+R_2} = 1666$[Ohm]. Furthermore, 0.883[Ohm]$\ll h_{ib} = 20$[Ohm]. Thus, all the design conditions established above are satisfied. The voltage v_o measured at the inductance terminals is shown in Fig. 9.45. The frequency measured in this experiment is 1.388[MHz].

The voltage v_o is shown in Fig. 9.46 when $R_t = 11000$[Ohm], which yields:

$$\frac{1}{R_{in}\frac{C_1+C_2}{C_1}}\left[\frac{1}{\frac{C_1^2}{R_{in}(C_1+C_2)^2}+\frac{1}{R_{ex}}+\frac{1}{R_{copper}}}\right]=1.0460. \tag{9.52}$$

This means that the loop gain is smaller. Note that having a smaller loop gain requires narrower oscillations; hence, a smaller incursion of the signal within the transistor nonlinear region to achieve a unit loop gain, i.e., to ensure sustained oscillations. Obtaining a larger oscillation amplitude in Fig. 9.45, when $R_t = 10000$[Ohm], is also explained in this manner. In fact, a slight distortion can be observed at the bottom part of the sinusoidal waveform when $R_t = 10000$[Ohm].

Finally, in Figs.9.47a, b and 9.48a, the polar plots are shown for $M(s)$, $Z_c(s)$ and $G(s)H(s)$ respectively, obtained with the numerical values referred to above and $R_t = 11000$[Ohm]. Note the similarities between Figs. 9.47a and 9.41b, and between Figs. 9.47b and 9.40b. Figures 9.42 and 9.48a are also very similar. The apparent differences for the frequencies close to zero are because such a part cannot be appreciated in Fig. 9.48a. This is verified in Fig. 9.48b, where a zoom-in is presented in Fig. 9.48a, and it is observed that the polar plot is tangent to the positive real axis in Fig. 9.42. It is observed in Fig. 9.48a that (9.52) is satisfied.

Figures 9.47a, b, 9.48a, and b were drawn using the following MATLAB code in an m-file:

```
beta=200;
RE=1e3;
R1=2e3;
R2=10e3;
L=0.328e-3;
Rcobre=101.677e3;
C1=27e-12;
C2=200e-12;
C3=0;
Rex=100*Rcobre;
Rt=10e3;
VT=0.026;
IEQ=1.3e-3;
hib=VT/IEQ
Rin=Rt+RE*hib/(RE+hib);
num=[Rin^2*C1*C2 Rin*C1 0];
den=[Rin^2*C2*(C1+C2) Rin*(2*C2+C1) 1];
M=tf(num,den)

numzc=[L*Rin*(C1+C2) L 0];
a3=(L*C1*C2+L*C3*(C1+C2))*Rin;
a2=L*C1+L*C3+(Rcobre+Rex)/(Rcobre*Rex)*L*Rin*(C1+C2);
```

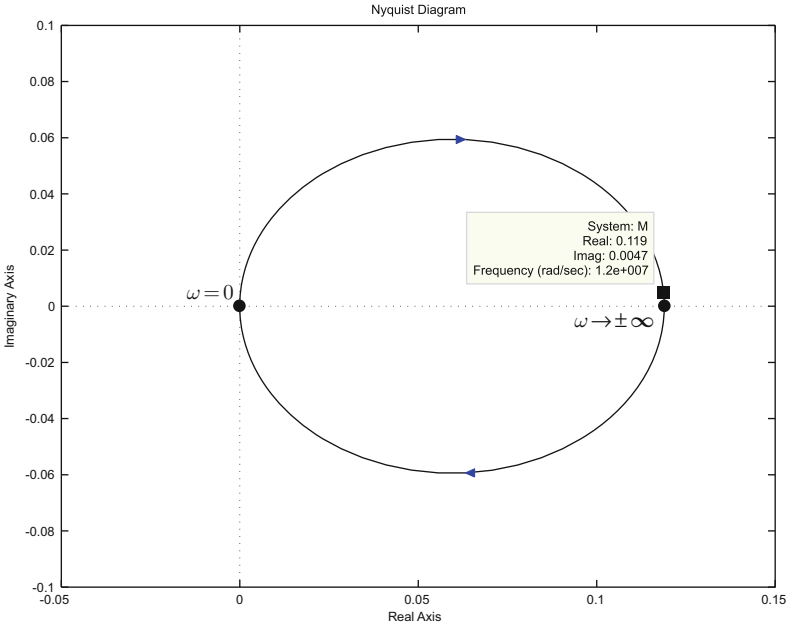

(a)

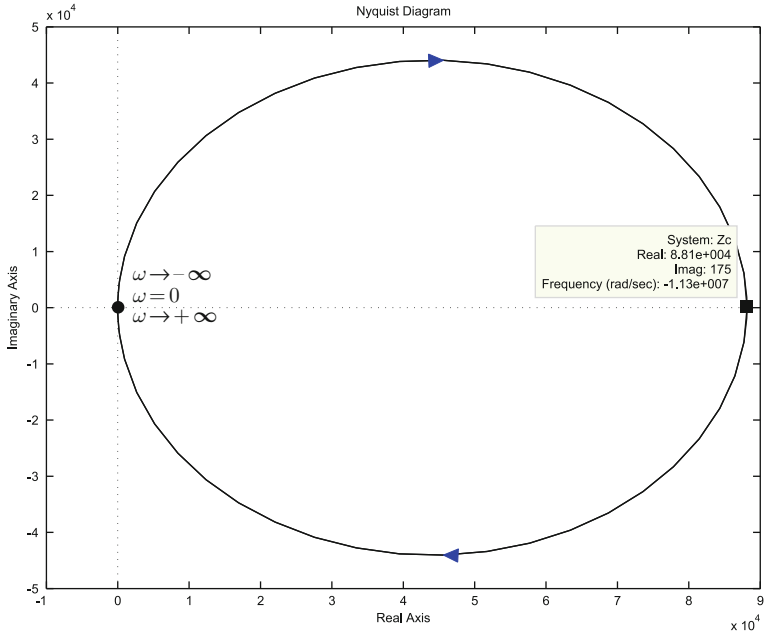

(b)

Fig. 9.47 Polar plots using the numerical values for the circuit experimentally tested . (**a**) $M(s)$. (**b**) $Z_c(s)$

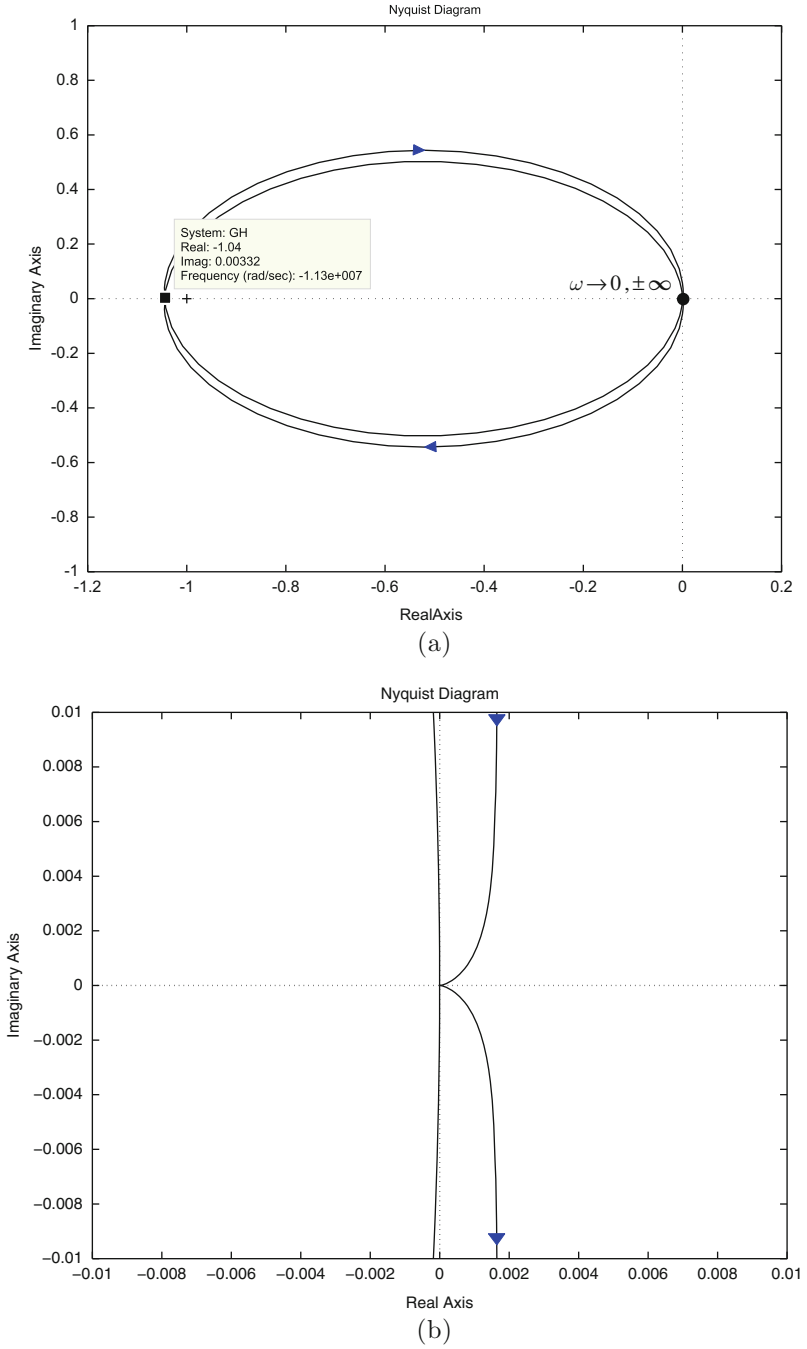

Fig. 9.48 Polar plots using the numerical values of the circuit experimentally tested (continued) . (**a**) $G(s)H(s)$. (**b**) $G(s)H(s)$ (zoom in)

```
a1=Rin*(C1+C2)+(Rcobre+Rex)/(Rcobre*Rex)*L;
denzc=[a3 a2 a1 1];
Zc=tf(numzc,denzc)

GH=-M*Zc/Rin

figure(1)
nyquist(M)
axis([-0.05 0.15 -0.1 0.1])

figure(2)
nyquist(Zc)

figure(3)
nyquist(GH)
axis([-.01 .01 -.01 .01])
w=1/sqrt(L*( C1*C2/(C1+C2)+C3 ))
f=w/(2*pi)
```

9.4 A Regenerative Radiofrequency Receiver

Regenerative radiofrequency (RF) receivers are recognized to possess very large gain. This is useful because radio signals collected in an antenna are very weak. This large amplification is achieved thanks to the use of positive feedback in the tuning circuit, as explained in this section.

The regenerative RF receiver depicted in Fig. 9.49 was introduced in [9]. The equivalent small-signal circuit is depicted in Fig. 9.50. This circuit is obtained by using the equivalent small-signal circuit for the transistor presented in Fig. 9.36a. From the circuit in Fig. 9.51a, the following is found:

$$\begin{aligned} v_r &= r_\pi i_b + v_1, \\ v_1 &= R_3 i_e = R_3(1+\beta) i_b, \end{aligned} \tag{9.53}$$

i.e.,

$$i_b = \frac{v_r}{r_\pi + R_3(1+\beta)}, \quad R = \frac{v_r}{i_b} = r_\pi + R_3(1+\beta).$$

Replacing this in (9.53), we obtain:

$$v_r = \frac{r_\pi}{r_\pi + R_3(1+\beta)} v_r + v_1,$$

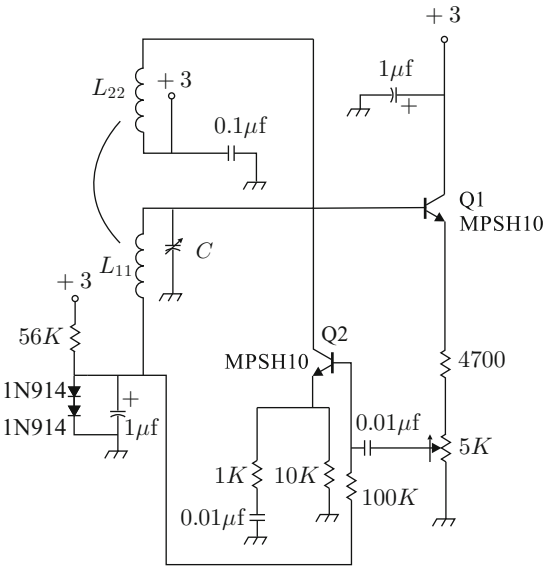

Fig. 9.49 A regenerative radio receiver

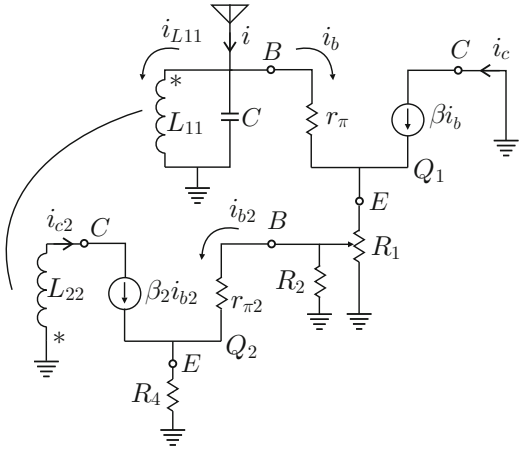

Fig. 9.50 Small-signal equivalent circuit for the receiver in Fig. 9.49

$$v_r \left(1 - \frac{r_\pi}{r_\pi + R_3(1+\beta)}\right) = v_1,$$
$$v_1 = \frac{R_3(1+\beta)}{r_\pi + R_3(1+\beta)} v_r. \tag{9.54}$$

On the other hand, from Fig. 9.51b, it is clear that:

$$R_3 = R_1(1-\alpha) + (\alpha R_1 || R_2 || z_{in}),$$

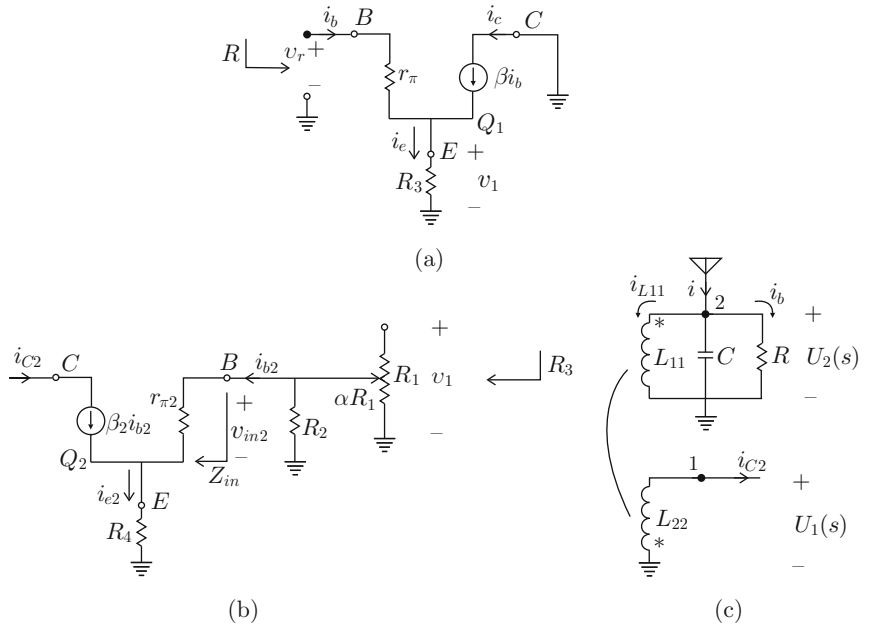

Fig. 9.51 Different sections of the circuit in Fig. 9.50 . (**a**) Transistor Q_1. (**b**) Transistor Q_2. (**c**) Tuning and feedback circuit

where $(\alpha R_1||R_2||z_{in})$ stands for the parallel equivalent resistance of αR_1, R_2, and z_{in}. Furthermore:

$$\begin{aligned} v_{in2} &= r_{\pi 2} i_{b2} + R_4 i_{e2}, \\ &= r_{\pi 2} i_{b2} + R_4(1+\beta_2) i_{b2}, \\ &= (r_{\pi 2} + R_4(1+\beta_2))\, i_{b2}, \\ z_{in} &= \frac{v_{in2}}{i_{b2}} = r_{\pi 2} + R_4(1+\beta_2). \end{aligned}$$

Moreover:

$$\begin{aligned} v_{in2} &= \frac{(\alpha R_1||R_2||z_{in})}{R_3} v_1 = z_{in} i_{b2}, \\ i_{b2} &= \frac{(\alpha R_1||R_2||z_{in})}{z_{in} R_3} v_1 = \frac{i_{c2}}{\beta_2}, \\ i_{c2} &= \beta_2 \frac{(\alpha R_1||R_2||z_{in})}{z_{in} R_3} v_1. \end{aligned} \tag{9.55}$$

Use of (9.54) and (9.55) yields:

$$i_{c2} = \gamma v_r, \quad \gamma = \beta_2 \frac{(\alpha R_1 || R_2 || z_{in})}{z_{in} R_3} \frac{R_3(1+\beta)}{r_\pi + R_3(1+\beta)}. \tag{9.56}$$

On the other hand, from Fig. 9.51c, the inductance matrix is found to be:

$$M = \begin{bmatrix} L_{11} & L_{12} \\ L_{21} & L_{22} \end{bmatrix},$$

because the arc depicted in Fig. 9.49 between L_{11} and L_{22} indicates that these coils are magnetically coupled. Note that according to Sect. D.2, in Appendix D:

$$L_{12} = L_{21} > 0,$$

because i_{L11} and i_{c2} enter into the inductances L_{11} and L_{22} respectively at the terminals with the polarity mark "$*$'.' This also means that the magnetic fluxes due to i_{L11} and i_{c2} have the same sense. This is a necessary condition for a successful operation of a regenerative RF receiver as it establishes positive feedback of the electric current from the collector of transistor Q_2 to the tuning circuit. Using (D.4), in Appendix D, i.e.,

$$\Gamma_{kj} = \frac{\text{cof}(M_{jk})}{\det(M)},$$

the invertances are computed to be:

$$\begin{aligned} \Gamma_{11} &= \frac{L_{22}}{L_{11}L_{22} - L_{12}L_{21}} > 0, \\ \Gamma_{22} &= \frac{L_{11}}{L_{11}L_{22} - L_{12}L_{21}} > 0, \\ \Gamma_{12} &= \frac{-L_{12}}{L_{11}L_{22} - L_{12}L_{21}} < 0, \\ \Gamma_{21} &= \frac{-L_{21}}{L_{11}L_{22} - L_{12}L_{21}} < 0, \\ \det(M) &= L_{11}L_{22} - L_{12}L_{21} > 0. \end{aligned} \tag{9.57}$$

Solving by nodes the circuit in Fig. 9.51c, the following is found:

$$I_{c2}(s) = \frac{\Gamma_{12}}{s} U_2(s) + \frac{\Gamma_{22}}{s} U_1(s), \tag{9.58}$$

$$I(s) = \left(sC + \frac{\Gamma_{11}}{s} + \frac{1}{R} \right) U_2(s) + \frac{\Gamma_{21}}{s} U_1(s), \tag{9.59}$$

where $U_1(s), U_2(s)$ are the Laplace transforms of voltages at nodes 1 and 2 respectively, as indicated in Fig. 9.51c, whereas $I_{c2}(s)$ and $I(s)$ are the Laplace

transforms of the collector current in the transistor Q_2, i.e., i_{c2}, and the electric current entering from the antenna, i.e., i respectively.

According to Fig. 9.51c and to the convention adopted to define the polarity marks in the coil terminals (see Sect. D.2, in Appendix D), if $U_2(s) > 0$ increases then the terminal with the polarity mark in the coil L_{22} is positive, producing a negative $I_{c2}(s)$, i.e., in the opposite direction defined for this current in Fig. 9.51c. This fact is correctly predicted by the term $\frac{\Gamma_{12}}{s}$ in (9.58), as $\Gamma_{12} < 0$. A similar argument justifies the term $\frac{\Gamma_{21}}{s}U_1(s)$ in (9.59), as $\Gamma_{21} < 0$ too.

Solving (9.58) for $U_1(s)$, replacing in (9.59), using definitions in (9.57) and rearranging, the following is found:

$$U_2(s) = \frac{\frac{1}{C}s}{s^2 + \frac{1}{RC}s + \frac{1}{L_{11}C}} \left(I(s) + \frac{L_{12}}{L_{11}} I_{c2}(s) \right).$$

As $U_2(s) = V_r(s)$, where $V_r(s) = \mathcal{L}\{v_r\}$, we can use (9.56) to obtain the block diagram in Fig. 9.52 and:

$$\frac{I_{c2}(s)}{I(s)} = \frac{\gamma \frac{1}{C}s}{s^2 + \left(\frac{1}{RC} - \gamma \frac{L_{12}}{L_{11}C} \right) s + \frac{1}{L_{11}C}}.$$

It is clear from Fig. 9.52 that positive feedback exists from the collector circuit of transistor Q_2 to the tuning circuit. Furthermore, it is interesting to observe that feedback is performed through the mutual inductance $L_{12} > 0$. This demonstrates that positive feedback is present thanks to the magnetic coupling between the inductances in the collector circuit of the transistor Q_2 and the tuning circuit.

Note that the transfer function:

$$G(s) = \frac{\gamma \frac{1}{C}s}{s^2 + \left(\frac{1}{RC} - \gamma \frac{L_{12}}{L_{11}C} \right) s + \frac{1}{L_{11}C}}, \tag{9.60}$$

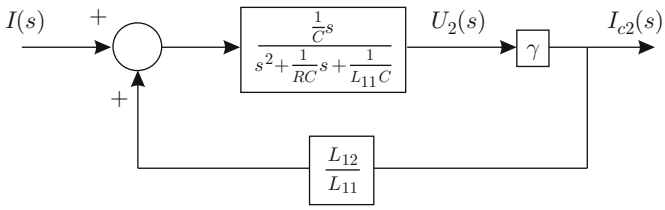

Fig. 9.52 Equivalent closed-loop block diagram of the circuit in Fig. 9.50

represents a *band-pass filter*, which has a very large gain when:

$$\omega \approx \sqrt{\frac{1}{L_{11}C}}, \quad \frac{1}{RC} - \gamma \frac{L_{12}}{L_{11}C} \approx 0,$$

i.e.,

$$|G(j\omega)|_{\omega=\sqrt{\frac{1}{L_{11}C}}} = \frac{\gamma \frac{1}{C}}{\frac{1}{RC} - \gamma \frac{L_{12}}{L_{11}C}} \to \infty, \quad \text{as } \left(\frac{1}{RC} - \gamma \frac{L_{12}}{L_{11}C}\right) \to 0.$$

Note that the last condition can be accomplished by suitably selecting γ, i.e., according to (9.56) by adjusting the potentiometer R_1, which implies modification of α. This explains why the regenerative receivers are recognized to have very large amplification gains. Moreover, it is recommended in the literature [10] to select the feedback gain of a regenerative receiver such as that obtained just before sustained oscillations appear. Note that $G(s)$ in (9.60) is a second-order system with zero damping if $\frac{1}{RC} - \gamma \frac{L_{12}}{L_{11}C} = 0$, which implies that sustained oscillations appear, even when $i = 0$. This, however, is not good for a regenerative receiver as these oscillations would dominate the circuit response; hence, the received radiofrequency signal could not be processed. On the other hand, if the feedback gain is chosen such that $\frac{1}{RC} - \gamma \frac{L_{12}}{L_{11}C} > 0$ is small, then sustained oscillations are avoided, i.e., the circuit is stable, but $|G(j\omega)|_{\omega=\sqrt{\frac{1}{L_{11}C}}}$ is still very large. Note that $\omega = \sqrt{\frac{1}{L_{11}C}}$ represents the frequency of the received signal that is selected to be processed, i.e., the frequency of the desired radio broadcast station.

For simulation purposes, the circuit in Fig. 9.49, introduced in [9], has the following numerical values: $L_{11} = 300 \times 10^{-6}$[H], $C = 100 \times 10^{-12}$[F], $L_{12} = 2 \times 10^{-6}$[H], $R_1 = 9.7$[KOhm], $R_2 = 100$[KOhm], $R_4 = 1000 \times 10 \times 10^3/(11 \times 10^3)$[OHm], $\beta = \beta_2 = 60$, $I_{BQ} = 10 \times 10^{-6}$[A]. This allows a radio signal of about 900[KHz] to be received. Using these values, we obtain the Bode diagrams presented in Figs. 9.53, 9.54, 9.55, for different values of α. Note that the magnitude of $G(j\omega)$ is greater than 30[dB] for all three values of α that have been tested. Moreover, for $\alpha = 0.2619$, the magnitude of $G(j\omega)$ is about 100[dB], which represents an amplification of about 10^5[A]/[A]. Thus, a very large gain is obtained in this case.

Figures 9.53, 9.54, and 9.55 were drawn by executing the following several times: MATLAB code in an m-file:

```
clc
clear all
L11=300e-6;
C=100e-12;
L12=2e-6;
R1=9.7e3;
```

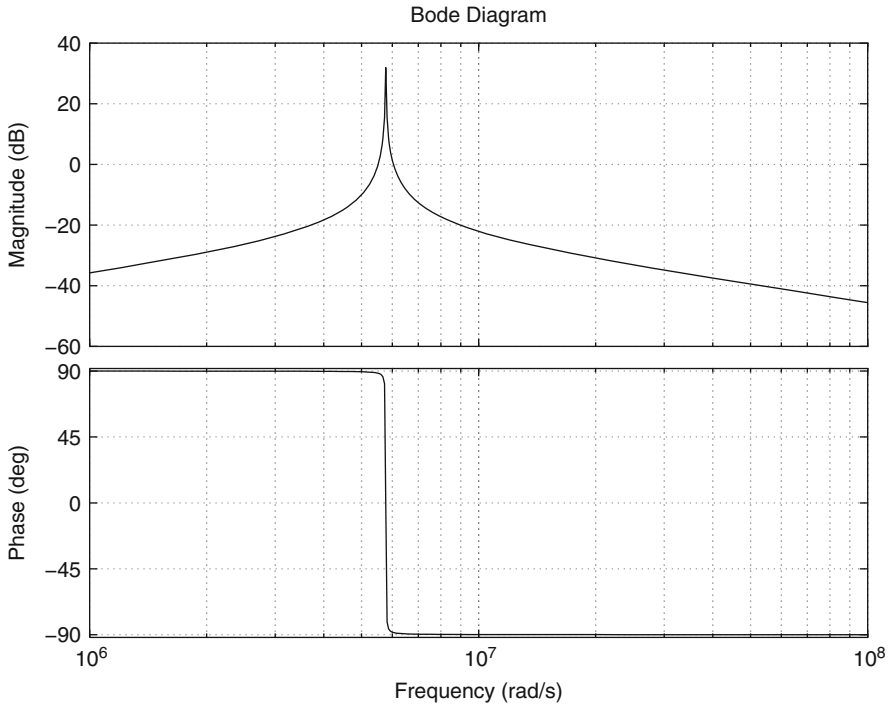

Fig. 9.53 Bode diagrams of $G(s)$ in (9.60) for $\alpha = 0.0515$

```
R2=100e3;
R4=1000*10e3/(11e3);
beta=60;
beta2=beta;
VT=0.026;
IBQ=10e-6;
rpi=VT/IBQ;
rpi2=rpi;
alfa=0.5/9.7%0.5/9.7%1.5/9.7%;%2.54/9.7;
zin=rpi2+R4*(1+beta2);
paralelo=1/( 1/(alfa*R1)+1/R2+1/zin );
R3=R1*(1-alfa)+paralelo;
gamma=beta2*paralelo/(zin*R3)*R3*(1+beta)/(rpi+R3*
    (1+beta));
R=rpi+R3*(1+beta);
G=tf([gamma/C 0],[1 1/(R*C)-gamma*L12/(L11*C)
1/(L11*C)]);
w=2.4e8:0.000001e8:3.4e8;
bode(G)
```

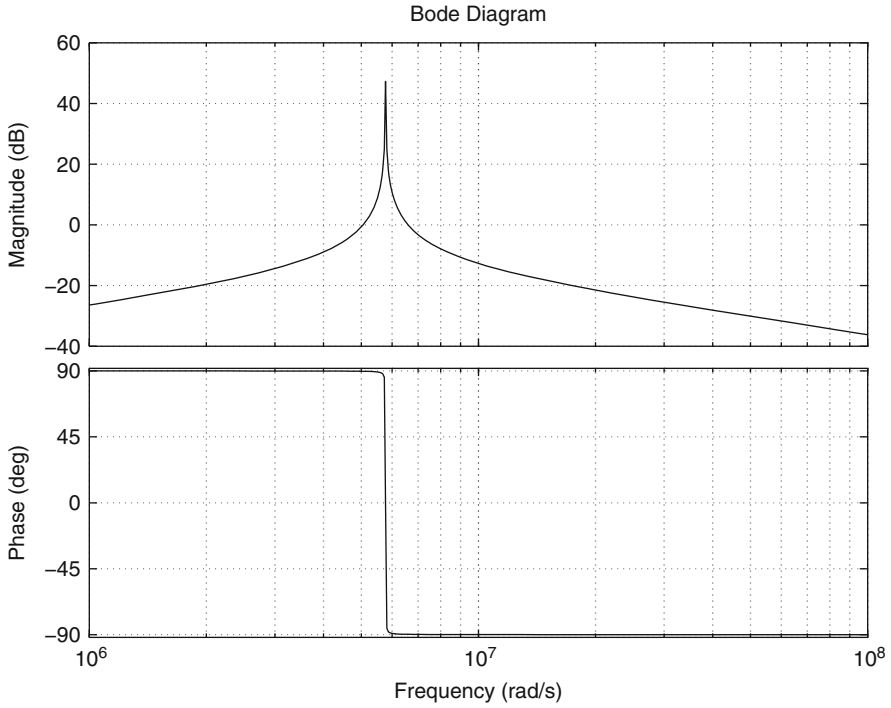

Fig. 9.54 Bode diagrams of $G(s)$ in (9.60) for $\alpha = 0.1546$

```
grid on
1/(R*C)-gamma*L12/(L11*C)
```

9.5 Summary

In this chapter, we have shown how to reduce the distortion produced by nonlinear electronic circuits, how to implement analog controllers in practice using feedback electronic circuits, and how to design and build electronic oscillator circuits producing a sinusoidal waveform. The fundamental tool for solving these problems is classical control, which includes the time response and the frequency response approaches.

In the case of reducing distortion in nonlinear electronic circuits, the basic idea is the use of feedback and a high loop gain to render the closed-loop system robust to open-loop system uncertainties, i.e., nonlinearities. No stability analysis is required for this solution because the circuits involved are assumed to have no dynamics, i.e., they can be modeled as static gains instead of differential equations.

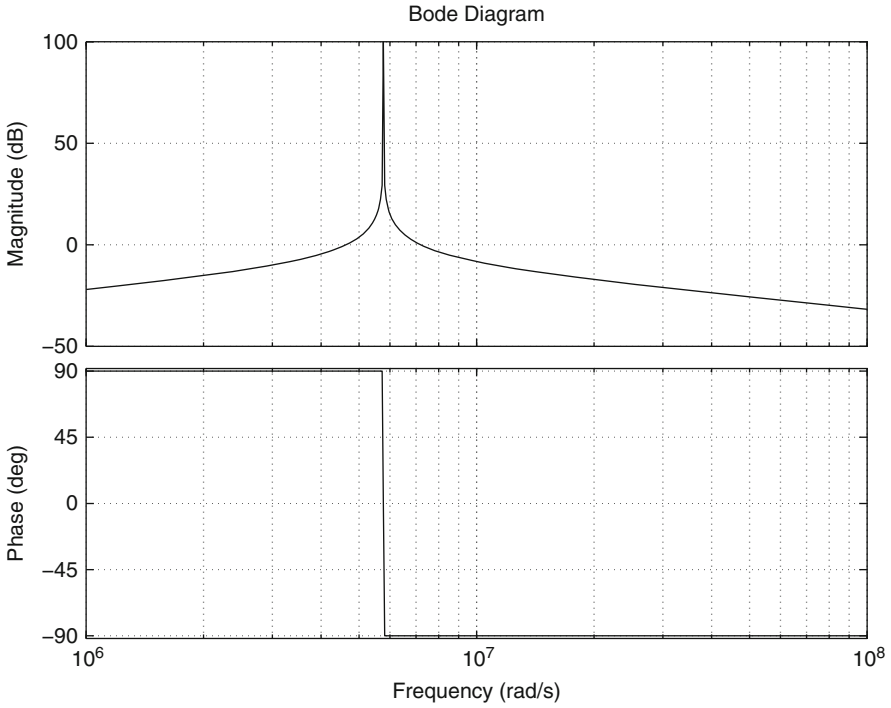

Fig. 9.55 Bode diagrams of $G(s)$ in (9.60) for $\alpha = 0.2619$

In the case of implementing analog controllers, it is important to choose an operational amplifier suitable for the particular application. Recall that the operational amplifier open-loop gain, designated by A_0 in the present chapter, is not really a constant, but it changes with frequency in a similar manner to the magnitude of a low-pass filter changing with frequency. This means that A_0 is reduced at high frequencies. Hence, an operational amplifier with a suitable bandwidth must be selected.

Finally, in the case of oscillator circuits, marginal stability is a fundamental concept. Hence, the circuit components must be chosen such that marginal stability is accomplished. The fundamental tools for analyzing and designing these circuits are the time response approach (location of closed-loop poles) in the case of operational amplifier-based circuits, and the frequency response approach (Nyquist stability criterion) in the case of bipolar transistor-based circuits.

9.6 Review Questions

1. When is a system marginally stable? Why is this concept important in the design of oscillator circuits?
2. Why is it said that it is not possible to design a completely linear oscillator circuit? Why does a nonlinear electronic circuit solve this problem?
3. A bipolar junction transistor is a nonlinear electronic device, then why are linear control techniques employed to design bipolar junction transistor-based oscillator circuits?
4. Why are Zener diodes required in operational amplifier-based oscillator circuits? Why are Zener diodes not employed in bipolar junction transistor-based oscillator circuits?
5. What is the so-called transistor small-signal model?
6. Why do you think oscillator circuits are positive feedback systems?
7. Why must an oscillator circuit be designed to be slightly unstable?

References

1. A. R. Hambley, *Electronics. A top-down approach to computer-aided circuit design*, Macmillan Publishing Company, New York, 1994.
2. R. F. Coughlin and F. F. Driscoll, *Operational amplifiers and linear integrated circuits*, 4th Edition, Prentice Hall, Englewood Cliffs, 1991.
3. N. S. Nise, *Control systems engineering*, 5th edition, John Wiley and Sons, New Jersey, 2008.
4. M. Alonso and E. J. Finn, *Physics*, Addison-Wesley, Reading, MA, 1992.
5. W. Hayward, *Introduction to radio frequency design*, The American Radio Relay League Inc., 1994.
6. P. H. Young, *Electronic communication techniques*, Merrill Publishing Company, 1990.
7. C. A. Desoer and E. S. Kuh, *Basic circuit theory*, International Student Edition, McGraw-Hill, Tokyo, 13th printing 1983.
8. M. Kaufman and A. H. Seidman, *Handbook of electronics calculations for engineers and technicians*, McGraw-Hill, USA, 1979.
9. R. Quan, *Build your own transistor radios*, McGraw-Hill, New York, 2013.
10. W. Hayward, R. Campbell, and B. Larkin, *Experimental methods is RF design*, The American Radio Relay League Inc., 2009.